Neurobiology of Disease

Distinct Features of Interictal Activity Predict Seizure Localization and Burden in a Mouse Model of Childhood Epilepsy

William F. Tobin[1] **and Matthew C. Weston**[1,2]

[1]Department of Neurological Sciences, University of Vermont, Burlington, VT 05405 and [2]Fralin Biomedical Research Institute and School of Neuroscience, Virginia Polytechnic and State University, Roanoke, VA 24016

The epileptic brain is distinguished by spontaneous seizures and interictal epileptiform discharges (IEDs). Basic patterns of mesoscale brain activity outside of seizures and IEDs are also frequently disrupted in the epileptic brain and likely influence disease symptoms, but are poorly understood. We aimed to quantify how interictal brain activity differs from that in healthy individuals, and identify what features of interictal activity influence seizure occurrence in a genetic mouse model of childhood epilepsy. Neural activity across the majority of the dorsal cortex was monitored with widefield Ca^{2+} imaging in mice of both sexes expressing a human *Kcnt1* variant (*Kcnt1*$^{m/m}$) and wild-type controls (WT). Ca^{2+} signals during seizures and interictal periods were classified according to their spatiotemporal features. We identified 52 spontaneous seizures, which emerged and propagated within a consistent set of susceptible cortical areas, and were predicted by a concentration of total cortical activity within the emergence zone. Outside of seizures and IEDs, similar events were detected in *Kcnt1*$^{m/m}$ and WT mice, suggesting that the spatial structure of interictal activity is similar. However, the rate of events whose spatial profile overlapped with where seizures and IEDs emerged was increased, and the characteristic global intensity of cortical activity in individual *Kcnt1*$^{m/m}$ mice predicted their epileptic activity burden. This suggests that cortical areas with excessive interictal activity are vulnerable to seizures, but epilepsy is not an inevitable outcome. Global scaling of the intensity of cortical activity below levels found in the healthy brain may provide a natural mechanism of seizure protection.

Key words: Ca^{2+} **imaging; genetic epilepsy KCNT1; mesoscale; seizures**

Significance Statement

Defining the scope and structure of an epilepsy-causing gene variant's effects on mesoscale brain activity constitutes a major contribution to our understanding of how epileptic brains differ from healthy brains, and informs the development of precision epilepsy therapies. We provide a clear roadmap for measuring how severely brain activity deviates from normal, not only in pathologically active areas, but across large portions of the brain and outside of epileptic activity. This will indicate where and how activity needs to be modulated to holistically restore normal function. It also has the potential to reveal unintended off-target treatment effects and facilitate therapy optimization to deliver maximal benefit with minimal side-effect potential.

Introduction

Many neurologic disorders are defined by the symptoms they produce, while the ways in which brain activity is disrupted in the disease state remain mysterious. This is particularly true for genetic epilepsies, which are often caused by variants in genes that encode common neuronal components (McTague et al., 2016). Because the neurophysiological role of these molecules depends on many factors, the effects of variants are potentially varied and widespread (Noebels, 2017). But, beyond the fact that they cause seizures and interictal spikes, little is known about how and where they reshape brain activity, and how this relates to disease symptoms. This is a critical knowledge gap for several reasons: (1) the subclinical effects of epileptogenic variants on neural activity may directly contribute to the occurrence of

Received Nov. 22, 2022; revised May 24, 2023; accepted June 5, 2023.

Author contributions: W.F.T. and M.C.W. designed research; W.F.T. performed research; W.F.T. analyzed data; W.F.T. and M.C.W. wrote the paper.

This work was supported by an American Epilepsy Society fellowship (W.F.T.) and National Institutes of Health Grants R01 NS110945 and NS130042 (to M.C.W.). We thank Todd Clason for his assistance with imaging equipment; Dr. Matt Mahoney for assistance with statistics, data analysis, and coding; Dr. Amy Shore for help with genotyping and manuscript editing; the Vermont Advanced Computing Center; members of the Weston lab and ECD group at the Univeristy of Vermont for their feedback; and Wayne Frankel and his group at Colombia for the Kcnt1 Y777H mouse line.

The authors declare no competing financial interests.

Correspondence should be addressed to Matthew C. Weston at mcweston7c@vtc.vt.edu.

https://doi.org/10.1523/JNEUROSCI.2205-22.2023

seizures and interictal spikes, (2) many epileptic patients suffer from neurologic co-morbidities that likely result from effects of the variant on brain activity outside of seizure epochs, and (3) the ideal therapeutic intervention would restore normal function in the diseased brain, not just stop seizures. However, without a comprehensive understanding of how disease alters brain activity, we cannot effectively design and evaluate treatments.

The *KCNT1* gene encodes a high conductance Na^+-activated K^+ channel, and *KCNT1* variants cause a spectrum of childhood epilepsies and neurodevelopmental disorders (Yuan et al., 2003; Heron et al., 2012; Møller et al., 2015; Ohba et al., 2015; Barcia et al., 2019). The KCNT1 channel is widely expressed in the brain and mediates a large, delayed, noninactivating, outward current that is engaged by Na^+ influx and depolarization (Bhattacharjee et al., 2002; Budelli et al., 2009; Rizzi et al., 2016; Saunders et al., 2018; Zeisel et al., 2018). In humans, the Y796H variant causes sleep-related hypermotor epilepsy [SHE; formerly autosomal dominant nocturnal frontal lobe epilepsy (ADFNLE); Plazzi et al., 1995; Heron et al., 2012; Mikati et al., 2015]. Aside from nocturnal seizures, patients carrying this variant exhibit a range of symptom severity, from nonambulatory and nonverbal to neurologically normal. Previously, we generated a mouse model in which the ortholog of the human Y796H variant (Y777H, or YH) replaced the wild-type (WT) allele (Shore et al., 2020). Mice homozygous for the YH allele show frequent spontaneous seizures, but normal lifespan and general health, making it an ideal model in which to monitor seizures and IEDs alongside interictal cortical activity.

Mesoscale Ca^{2+} imaging allows measurement of bulk neural activity at centimeter scale with high spatial resolution (~25 μm) across the entire dorsal cortex of awake and behaving mice (Wekselblatt et al., 2016). It has been used in healthy mice to identify neural correlates of sensory stimulation, movement, and learning and memory (Makino et al., 2017; Gilad et al., 2018; Musall et al., 2019; Pinto et al., 2019; Jacobs et al., 2020; Salkoff et al., 2020; Zatka-Haas et al., 2021). It is also well-suited to the study of epileptic pathology, which may involve brain-wide networks of connected areas, because it offers superior spatial resolution and a more linear relationship to neuronal activity relative to alternatives at this scale (e.g., EEG, fMRI; Rossi et al., 2018). Previous studies used this approach to image pharmacologically-induced focal seizures and IEDs in WT rodents (Daniel et al., 2015; Baird-Daniel et al., 2017; Rossi et al., 2017; Liou et al., 2018), and epileptic activity caused by glioma (Hatcher et al., 2020; Montgomery et al., 2020), and provided key insights into seizure propagation.

Genetic epilepsy models, however, offer the opportunity not only to study spontaneous seizures, which may significantly differ from those induced by acute chemoconvulsants, but also the natural interictal brain activity from which seizures arise. Here, we imaged both of these activity regimes at the mesoscale using GCaMP6 fluorescence. Categorizing interictal cortical events by their spatial profile allowed us to compare equivalent types of activity across genotypes, revealing a surprising degree of variety and divergence in the variant's effects across both cortical areas and individuals. Importantly, this variation was systematically related to patterns of epileptic pathology in mutant mice, demonstrating previously unappreciated links between ictal and interictal activity.

Materials and Methods

Mice

The animals included in this study were housed and used in compliance with the National Institutes of Health *Guidelines for the Care and Use of Laboratory Animals* and approved by the Institutional Animal Care and Use Committee at the University of Vermont. Experimental mice of either sex were generated by first mating the *Kcnt1*^{Y777H} knock-in line (Shore et al., 2020) to the *Snap25*-GCaMP6s line (The Jackson Laboratory stock #025111; Madisen et al., 2015). Double heterozygous offspring were then mated to generate mice carrying the *Snap25*-GCaMP6s construct that were either homozygous Y777H or WT at the *Kcnt1* locus. *Kcnt1*^{Y777H} genotyping was performed as previously reported (Shore et al., 2020), and *Snap25*-GCaMP6s was genotyped following the protocol supplied by Jackson Labs.

Surgery

All surgical procedures were performed on mice under 1–2% isofluorane anesthesia. The mouse's eyes were coated with protective ophthalmic ointment (Paralube, Dechra Pharmaceuticals) and scalp hair removed, before fixing the head in a stereotaxic frame (Stoelting, Mouse and Neonates Adaptor, item #51625) and placing a homeothermically controlled heating pad under the body (PhysioSuite, Kent Scientific, item #PS-02). Before removing the scalp skin with fine surgical scissors (FST item no. 14058-09), it was scrubbed with 10% povidone-iodine followed by 70% ethanol, three times. Once the skull was exposed and overlying fascia removed, neck muscles were retracted, bilaterally, at their anterior most attachment point on the interparietal bone. Marginal, cut skin was glued in place with tissue adhesive (3M Vetbond). For one animal, the dorsal cranium was replaced with a large glass window (Crystal Skull, Labmaker) following the protocol detailed previously (Kim et al., 2016). Next, an aluminum head plate, fabricated following a design previously shown (Goldey et al., 2014), was fixed to the skull using UV curing cyanoacrylate (Loctite 4305). To minimize the escape of excitation light from the implant during imaging, powdered black tempera paint (Jack Richeson & Co SKU #101508) was mixed into the glue before curing. For transcranial imaging, a thin layer of UV curing cyanoacrylate was applied to the surface of the skull. After surgery, the head plate was filled with silicone elastomer (Kwik-Sil, WPI) for protection during recovery. Dual antibiotic and anesthetic cream (Neosporin Plus) and ketoprofen (5 mg/kg, i.p.) were administered.

Data acquisition

We used a custom tandem-lens epifluorescent macroscope (Ratzlaff and Grinvald, 1991) with 50- and 105-mm focal length objective and image forming lenses, respectively (Nikon Nikkor 50 mm f/1.4 and 105 mm f/1.8), and a broadband LED (X-Cite 120 LED) with a GFP filter set (Chroma 49002) in 50-mm circular glass, mounted in Thorlabs SM2 hardware in the configuration illustrated in Figure 1*A*. In most sessions, a 530-nm LED (Thorlabs, M530F2, LEDD1B) coupled to an optical fiber was pointed obliquely at the cortical surface to illuminate every other frame to correct for hemodynamic artifacts. We included seizure data from sessions lacking reflectance images in the study but excluded these sessions from analyses involving comparison of interictal events across mice, as a fair comparison of event duration and intensity was not possible between imaging conditions. All images were captured at 20 Hz (reflectance and GCaMP) with an Andor Zyla 5.5 sCMOS camera (Camera Link 10-tap) controlled by μManager software (Edelstein et al., 2014; version 1.4) within MATLAB. Mice were secured under the objective lens and supported by a treadwheel made from a Styrofoam cylinder; wheel position was recorded with an optical shaft encoder (US Digital) and a PCIe DAQ system (National Instruments). Video of the mouse's body was collected under infrared illumination (Camera: Allied Vision GC750). No habituation process was employed; data collection began the first time each mouse was placed on the treadwheel and typically consisted of 30 min imaging sessions, once a day. The six *Kcnt1*$^{m/m}$ mice in the study were imaged individual mice for 11, 1, 11, 9, 4, and 3 d, respectively, typically during 30-min sessions each day. The four WT mice in the study were imaged for 10, 9, 4, and 4 d, respectively, also over 30-min sessions.

Image processing

All data processing was performed using MATLAB, either on the acquisition PC or through the Vermont Advanced Computing Center. Raw

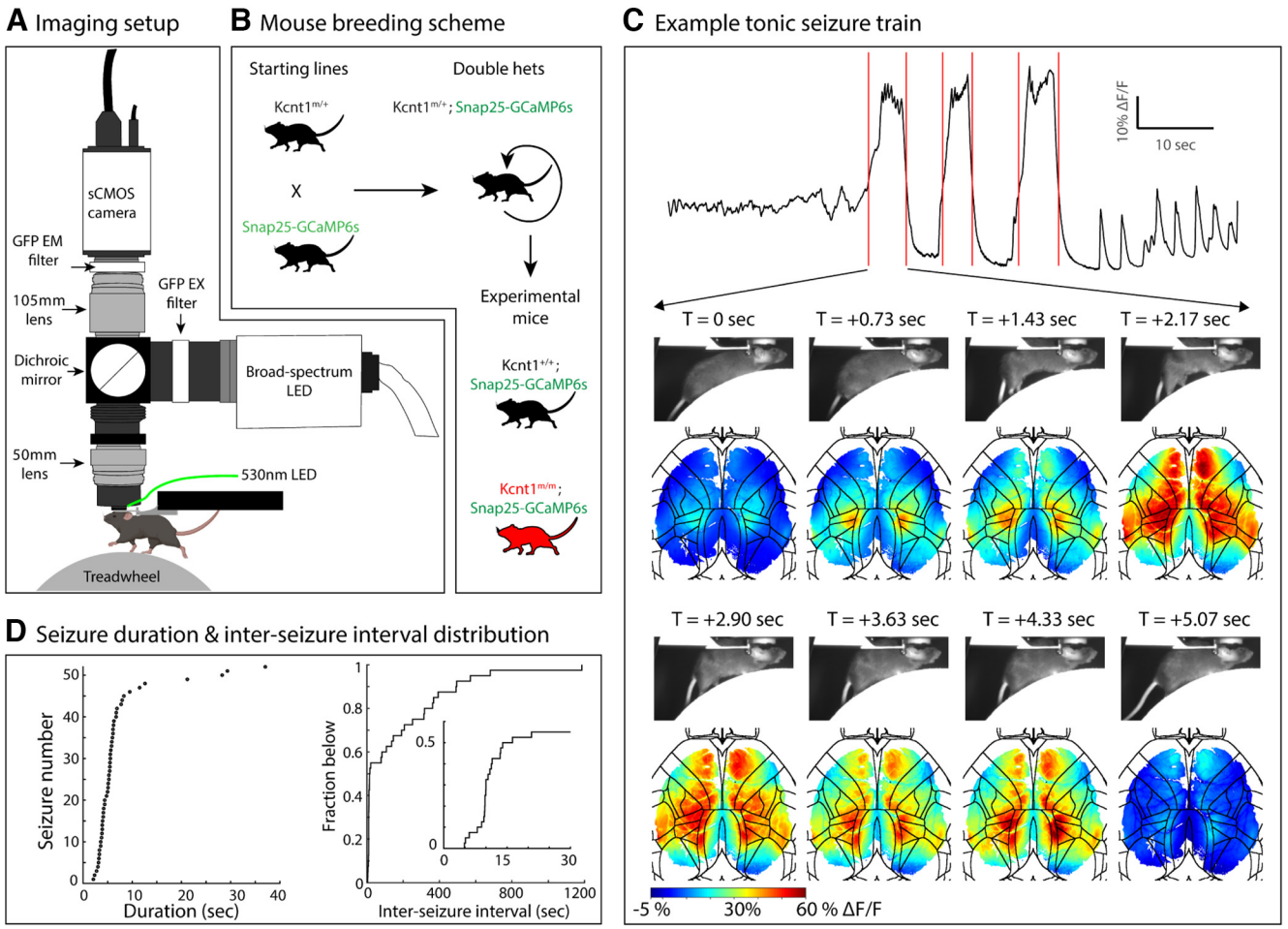

Figure 1. Widefield imaging of dorsal cortex in *Kcnt1*$^{m/m}$ and WT mice. ***A***, A schematic of the tandem-lens, epifluorescent macroscope used for *in vivo*, awake widefield Ca^{2+} imaging. Every other frame was illuminated with a 530-nm LED pointed obliquely at the skull surface; the resulting reflectance images were used to correct our GCaMP6s signal for hemodynamic artifacts. ***B***, The breeding scheme used to generate experimental mice. ***C***, An example tonic seizure train. The trace shows average ΔF/F signal calculated across all pixels involved in at least one of the three seizures shown. Red lines demarcate seizure boundaries. Images below show still frames of mouse body video and simultaneous ΔF/F frames of the dorsal cortex, with black lines marking the Allen Mouse CCF area borders. Time relative to seizure start is indicated above each pair of frames. ***D***, Most seizures were brief and clustered in time. The scatter plot on the left shows the duration of all seizures. The plot on the right displays an empirical cumulative distribution function of interseizure interval generated from all sessions containing more than one seizure. The inset shows a zoom to the foot of the plot.

images were saved as TIFF files. Image processing was performed in the following steps. (1) A dark frame was subtracted from all illuminated frames before we deinterleaved reflectance and epifluorescence images. (2) Raw GCaMP6s fluorescence values from each pixel in the epifluorescence images were transformed into ΔF/F values, using the pixel's average value over the bottom 20% of raw values as an estimate of baseline fluorescence. (3) To correct for hemodynamic artifacts, we calculated the fractional change in reflected fluorescence collected under 530-nm LED illumination on each pixel as $(Ref-Ref_o)/Ref_o$, using the pixels average value as Ref_o. This was then subtracted from GCaMP6s ΔF/F. (4) As a final denoising and data compression step, we performed singular value decomposition (SVD) on ΔF/F stacks, using code adapted previously published work (Steinmetz and Peters, 2019). The resulting right singular vectors were detrended and filtered. Detrending was performed with the MATLAB built-in function detrend ('linear'), a second order Butterworth band stop with 7- and 14-Hz cutoffs was applied to suppress the heartbeat artifact, as well as a second order high pass Butterworth with 0.01-Hz cutoff to remove slow fluorescence fluctuations. (5) A rank-50 reconstruction of frames was produced and used for all analyses. In three imaging sessions, seizure activity transitioned to cortical spreading depression (CSD); CSD activity was removed before performing SVD because it distorted the resulting singular vectors/values.

Seizure identification

To identify seizures, periods in which cortical activity was high and changing rapidly were detected using two vectors: (1) the fraction of pixels above 20% ΔF/F in each frame and (2) the average pixel-wise ΔF/F difference between successive frames. After smoothing both with a 10-s moving average filter, we detected coincident peaks (within 15 s) in the envelope of vector (1) and vector (2) using the MATLAB built-in function findpeaks(). Potential seizures were then screened for behavioral symptoms by comparing body videos and cortical ΔF/F. Borders of seizure activity were determined using a per-animal ΔF/F threshold set to the 99th percentile of nonseizure, non-IED, interictal cortical activity event peaks (see below). For each seizure, we recorded the first frame in which at least 1% of pixels were above threshold (seizure start), the first frame in which the number of pixels above threshold was maximal (end of seizure growth phase), and the first trailing frame in which <1% of pixels was above threshold (seizure termination). Because IEDs sometimes occurred close to seizures and involved above-threshold activity, any "seizures" that met our IED criteria were eliminated. To ensure that spatial maps of seizure onset and spread were not overly influenced by light scattering through tissue or skull, spatial patterns in seizure recruitment were also calculated by scaling seizure thresholds by F_0 on each pixel. Spatial patterns of seizure recruitment calculated in this manner were similar to unscaled patterns. Recruitment patterns in the one mouse with a glass window were also similar to those with intact skulls (Fig. 4), suggesting that these patterns were not compromised by light scattering.

Image alignment and registration

A nonreflective similarity transformation based on manually placed control points was used to register images from each session to the Allen

Mouse Common Coordinate Framework (CCF) v3 (Allen et al., 2017; Musall et al., 2019). Images from all sessions were co-registered with a three-step process. For step 1, we performed a within-animal affine transformation based on histogram equalized session average GCaMP6s images. For step 2, we performed an across-animal registration based on the functional topography revealed by seed pixel correlation maps (SPCMs; code adapted from Steinmetz and Peters, 2019). For each session, we generated SPCMs using a 50-by-50 grid of seed pixels, calculated the average map from seed pixels in primary visual cortex (VISp), and took the grand average across all sessions from a given mouse. We used these to identify a similarity transformation to align images across mice. For step 3, the cross-animal registration was refined by calculating another similarity transformation based on each mouse's grand average VISp SPCM and an average VISp SPCM taken across mice following the second step.

Long-range seizure jump identification

To identify long-range jumps in seizure propagation, we used the MATLAB built-in function imextendedmin() on seizure recruitment rank maps after preprocessing with the following steps: (1) Set the value of all pixels outside the brain to the average value of brain pixels, (2) Interpolate over gaps corresponding to surface vasculature using the built-in MATLAB function regionfill(), and (3) Filter the image with a Gaussian smoothing kernel with a SD of 4.

Preseizure image template matching

To generate preseizure activity templates, we processed each preseizure frame using the same three steps described in the previous section. The template was a binary mask covering the top 5% of pixel values in the resulting image. We created equivalent templates using the single frame in which activity was most widespread during each detected interictal event and calculated a "match score" between each preseizure template and all interictal event frame templates. This score was the number of overlapping template pixels divided by the total number of pixels in the smaller mask. To generate the null distribution of interictal event template overlap scores, we repeated this process using templates derived from interictal events belonging to one of the 10 major event types (Fig. 4) in place of preseizure activity patterns.

To compare peak activity localization preceding seizure onset to interictal occurrences of similar activity, we calculated a template match score between each preseizure activity pattern and all other frames captured during seizure, IED, and running-free periods in the mouse that produced the preseizure activity pattern (source mouse). To construct the null distribution of match scores preceding top interictal matches (Fig. 6*E*,*F*), we randomly selected an interictal match from among its top 50 best matches, averaged individual match score traces 20 s before each interictal match frame, and repeated this process 500 times to estimate 95% confidence interval (CI). To control for the fact that preseizure match scores come from templates derived from preseizure frames, not interictal match frames, we used templates derived from each interictal match frame in constructing our null.

Event detection, peak intensity, and duration measurement

We performed event detection in two steps. (1) For each session, we calculated average ΔF/F within regions of interest (ROIs) covering the FOV in a 50-by-50 grid and detected peaks in these signals using the MATLAB built-in function findpeaks() with a 7.5% prominence threshold. Events in separate ROIs occurring within 250 ms of each other were considered parts of the same event. (2) We reconstructed pixels and frames encompassing each event at full resolution and repeated findpeaks() using the same threshold on each pixel's ΔF/F values.

We measured event peak intensity (Fig. 8) from images in which each pixel was assigned its ΔF/F peak prominence value. After smoothing with a 2D Gaussian filter ($\sigma = 1$) we identified 2D peaks (Natan, 2021) and used the highest value. To measure event duration, we used images in which each pixel was assigned its width-at-half-max value and smoothed with the same filter as intensity images. Event duration was taken as the value in this image at the same location as event peak intensity

Clustering

Hierarchical clustering was performed on the CCF area average peak ΔF/F vectors. All interictal events, from both genotypes, were pooled before calculating a cluster tree with the MATLAB built-in function linkage() based on the average correlation distance between clusters. To decide how many clusters to consider, we used a silhouette analysis. In the case of IEDs, a two-cluster solution produced the highest silhouette value, so the highest local maximum was used, which was found at nine clusters. In the case of non-IED events, a global maximum was identified at 20 clusters.

Statistical analyses

The permutation test we used to establish significance of results in Figure 5 is described in the figure legend. The confidence intervals used to establish significance of results in Figure 6 are described above in the section Preseizure image template matching. To test for group differences in interictal activity event rate and duration (Fig. 7), we shuffled and re-drew session event rates or durations for each cluster 1,000,000 times. We then calculated a *p*-value as the fraction of shuffles generating a group difference more extreme than that seen in the true arrangement. These *p*-values were corrected for multiple comparisons using the Holm–Bonferroni method (Groppe, 2023; $n = 10$ tests).

Results

Widefield imaging of the dorsal cortex in *Kcnt1*$^{m/m}$ and WT mice

To understand how a *KCNT1* variant alters brain activity at the mesoscopic scale, we performed widefield Ca^{2+} imaging of the dorsal cortex in *Kcnt1*$^{m/m}$ and WT mice (Fig. 1*A*,*B*). We measured seizures, IEDs, and interictal cortical activity (all activity outside of seizures and IEDs in both *Kcnt1*$^{m/m}$ and WT mice). Experimental mice were generated by crossing a line carrying the Y777H *KCNT1* variant (corresponding to human Y796H) to the *Snap25*-2A-GCaMP6s knock-in line, in which GCaMP6s is expressed in all neurons (Fig. 1*B*; Madisen et al., 2015). To gain optical access to the cortex, we either removed the dorsal skull, implanting a glass cranial window ($n = 1$ *Kcnt1*$^{m/m}$), or rendered the bone semi-transparent with a layer of cyanoacrylate ($n = 4$ WT, $n = 5$ *Kcnt1*$^{m/m}$; Kim et al., 2016; Shore et al., 2020). We then imaged cortical GCaMP6s fluorescence with a custom tandem-lens epifluorescent macroscope (Ratzlaff and Grinvald, 1991; Wekselblatt et al., 2016) while mice were awake and free to run on a Styrofoam treadwheel (Fig. 1*A*). In addition to cortical imaging, we recorded treadwheel motion and body video during each session. In total, we collected 34.5 h of imaging data, 21 h from six *Kcnt1*$^{m/m}$ mice and 13.5 h from four WT mice.

Spontaneous seizure mapping identifies seizure susceptible cortical areas

Previously, using video-EEG monitoring, we showed that *Kcnt1*$^{m/m}$ mice have two types of spontaneous seizures: generalized tonic-clonic (lasting 30–60 s), and tonic (≈5 s, often occurs in trains; Shore et al., 2020). In the widefield imaging data, seizures were identified as abnormally high GCaMP6s fluorescence occurring simultaneously with behavioral seizure correlates, such as Straub tail, back arching, and convulsions (Fig. 1*C*; Movie 1). We identified 52 seizures in four of six *Kcnt1*$^{m/m}$ mice. Most were brief (median duration 4.525 s) and occurred in trains (median interseizure interval 13.825 s; Fig. 1*D*), suggesting that they corresponded to the tonic seizures identified by video-EEG.

To map seizure emergence and propagation, we determined the time at which signals on each pixel first crossed seizure threshold (see Seizure Identification). We then defined the

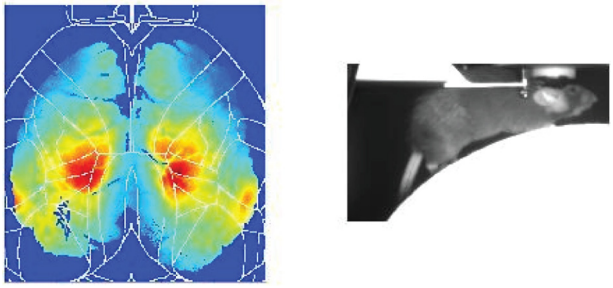

Movie 1. Example video of simultaneous widefield Ca^{2+} signal and mouse body movements. The video shows the simultaneous widefield fluorescence signal (left) and mouse body (right). The video contains three tonic seizures, the first of which begins at ≈17 s. There is a buildup of the Ca^{2+} signal in the impending emergence zone over the ≈10 s prior to seizure onset. [View online]

seizure "emergence zone" as the group of pixels above threshold in the first frame of each seizure (Fig. 2*A*,*B*). These areas ranged in size from 0.0026 to 0.93 mm^2 (mean ± SEM, 0.28 ± 0.0287 mm^2), were mostly (65%) bilaterally symmetrical (Fig. 2*A*) and only rarely (17%) involved discontinuous patches, separated by >300 μm in the same hemisphere.

We localized emergence zones to cortical areas by aligning our images to the Allen Mouse Common Coordinate Framework v3 (CCF) and measuring the fraction of each emergence zone in each area in our field of view (FOV; Fig. 2*A*–*C*; Wang et al., 2020). Seizures most often emerged in a region where the anterior visual [VISa; a constituent of posterior parietal cortex (PTLp)], retrosplenial (RSP), and anteromedial visual (VISam) area borders converge, which we call the posterior emergence zone (PEZ). This location is illustrated by the example emergence zone in Figure 2*A*, peak values in the Figure 2*B* heatmap, and as seizures 1–13 in the Figure 2*C* heatmap. The second most common emergence zone was medial secondary motor cortex (MOs), as illustrated in seizures 36–52 in Figure 2*C*.

Following emergence, seizures expanded in the cortex following a roughly sigmoidal growth curve (Fig. 2*D*), reaching maximum sizes of ~9–24 mm^2 (upper limit reflects the size of our FOV). Growth rate was variable across seizures, and some of this variation was systematic; seizures that emerged shortly after another seizure ended grew much more rapidly than others.

To visualize seizure propagation, we ranked the time at which pixels entered each seizure and created rank maps (Fig. 2*E*,*F*). These showed that seizures followed a predictable pattern in their spread; the earliest recruited areas were those that served as emergence zones during other seizures. This is illustrated by comparing the example emergence and recruitment rank maps (Fig. 2*A*,*E*); following emergence at the PEZ, distant medial MOs was recruited before much closer areas such as the primary visual (VISp) and barrel (SSp-bfd) cortices. Collectively, the areas prone to both seizure emergence and early recruitment included medial MOs, lateral RSP, PTLp (comprised of VISa and rostrolateral visual area, VISrl), VISam, SSp-tr, and the most posteromedial corner of MOp, which links the anterior and posterior portions of this set (Fig. 2*F*). These areas also showed the most intense seizure-related activity (Fig. 2*G*) and the longest seizure durations (Fig. 2*H*). Taken together, these data argue that not all cortical areas in *Kcnt1*$^{m/m}$ mice are equally susceptible to seizures; a consistent subset is most likely to host emergence, get recruited early, and show the most intense and longest duration activity during seizures.

Cortical areas susceptible to seizures and IEDs show partial overlap

In addition to seizures, interictal epileptiform discharges (IEDs), or interictal spikes, are another signature form of pathologic neural activity observed in the epileptic brain. We next investigated whether these events also localized to specific cortical areas, and how their localization compared with seizures. In mesoscale Ca^{2+} imaging data, IEDs are distinguished by their abnormally high intensity and brief duration (Rossi et al., 2017; Steinmetz et al., 2017; Shore et al., 2020). To map IEDs, we first identified events in *Kcnt1*$^{m/m}$ and WT cortical activity during seizure-free, nonrunning periods by detecting ΔF/F peaks that exceeded a prominence threshold of 7.5% (see Event detection, peak intensity, and duration measurement). All brief events (<0.875 s mean width at half peak) with unusually high peak intensity (>99th percentile for WT event prominence) were categorized as IEDs (Steinmetz et al., 2017). We detected many IEDs in *Kcnt1*$^{m/m}$ mice that appeared in a scatter plot of event intensity versus duration as a lobe of points not seen in WT mice (Fig. 3*A*, *B*, magenta points). The frequency of IEDs in individual *Kcnt1*$^{m/m}$ mice varied greatly (range: 0.42×10^{-3} to 113.8×10^{-3} Hz), with the two mice with lowest IED frequency being the same two in which we did not observe seizures. Interestingly, IEDs did not appear as a distinct cluster of points in the *Kcnt1*$^{m/m}$ plot, but rather a continuous extension of the point cloud (Fig. 3*A*), suggesting that the IED/non-IED distinction may not correspond to any natural division among cortical events, and that *Kcnt1*$^{m/m}$ interictal activity may occur along a gradient spanning normal and pathologic.

To localize *Kcnt1*$^{m/m}$ IEDs, we measured the average peak ΔF/F in each cortical area for every IED, and then grouped IEDs with similar spatial profiles using hierarchical clustering (Fig. 3*C*; see Clustering). Most *Kcnt1*$^{m/m}$ IEDs had peak activity in MOs; however, they also variably involved lower levels of activation in primary motor cortex (MOp), adjacent primary somatosensory (SSp) regions, and PTLp (Fig. 3*C*, first, third, and fourth largest clusters). Another large population of IEDs showed peak activity in posterior retrosplenial cortex (RSP), extending into adjacent higher visual areas and posterior MOs (Fig. 3*C*, second largest cluster). Together, these four clusters represent almost 90% of IEDs.

As in the case of seizures, these data show strong biases in IED vulnerability among cortical areas in *Kcnt1*$^{m/m}$ mice. The most susceptible region was MOs, which was also highly susceptible to seizure. However, as can be seen by comparing maps of seizure recruitment to the average IED rate in each individual animal (Fig. 4), even these areas within MOs are not completely overlapping. Apart from MOs, seizure and IED-susceptible regions were largely nonoverlapping. For instance, although RSP was prone to both, the subregions involved in each appeared distinct (Figs. 2*B*, 3*C*). Importantly, we did not find an IED cluster with peak activity at the most frequent seizure emergence site, the PEZ (Figs. 2*B*, 3*C*), suggesting that the neural population most likely to host seizure emergence is not notably susceptible to IEDs.

Mesoscale interictal activity is comprised of event types with equivalent spatial structure in *Kcnt1*$^{m/m}$ and WT mice

Having mapped spontaneous seizures and IEDs, we next mapped interictal activity in *Kcnt1*$^{m/m}$ and compared it to that of WT mice. To do this, we calculated the average event-related peak intensity by cortical area for each event outside of seizure, IED, and treadmill movement (event detection described above; see Event detection, peak intensity, and duration measurement). As

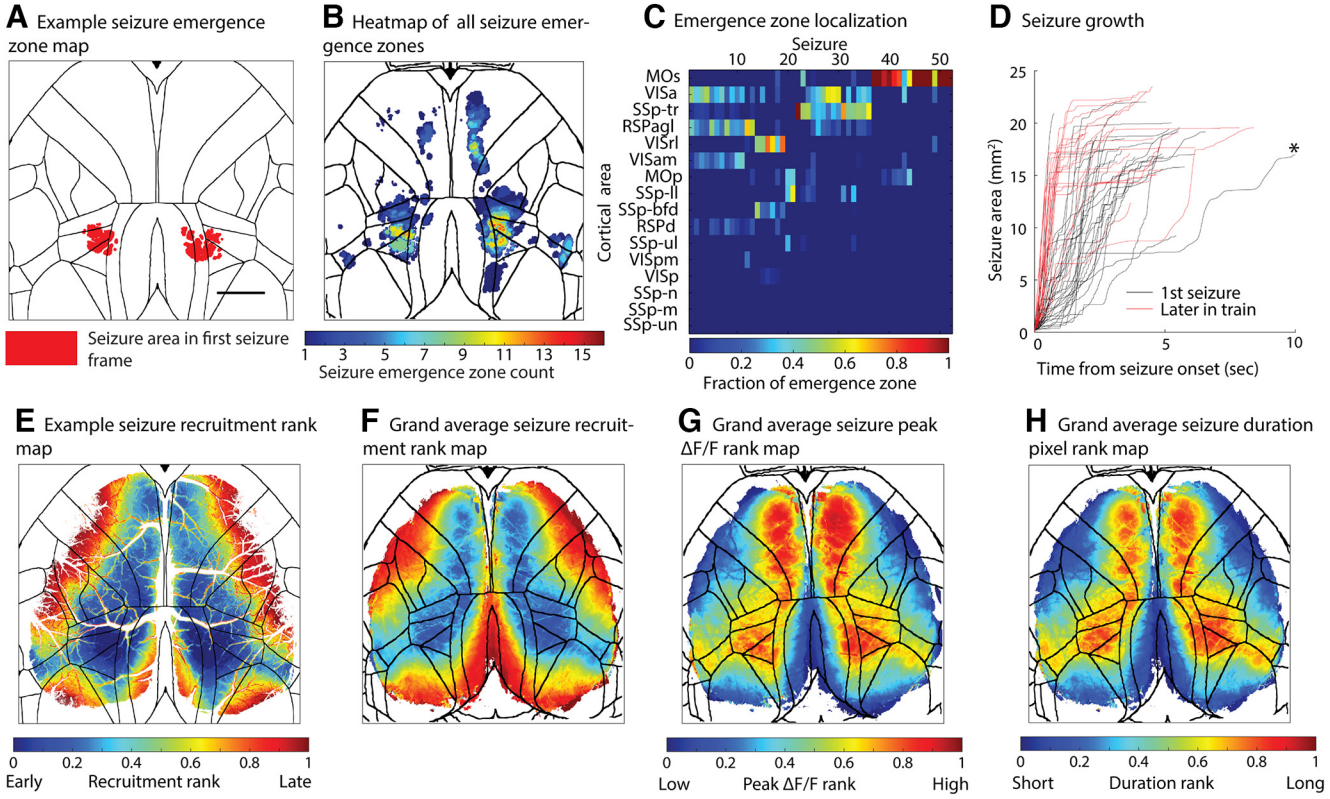

Figure 2. Spontaneous seizure mapping identifies seizure susceptible cortical areas. ***A***, An example seizure emergence zone map. Red pixels are those above seizure threshold in the first frame containing seizure activity. Black lines mark the borders of the Allen Mouse CCF areas. Scale bar is 1 mm. ***B***, A heatmap of seizure emergence zones summed over all 52 seizures. The value of each pixel indicates the number of seizures in which that pixel was a part of the emergence zone. ***C***, A heatmap showing the fraction of each emergence zone located within each of the 16 CCF areas imaged in all sessions. ***D***, A plot showing the area of seizing tissue as a function of time, covering the period between the first seizure frame and maximal seizure area. Black traces represent the first seizure in seizure trains or seizures that occurred singly, and red traces the seizures that occurred after the first in seizure trains. Asterisk marks a single trace that extended beyond the limit of the *x*-axis. ***E***, An example seizure recruitment rank heatmap (same seizure as panel ***A***). The value of each pixel is its recruitment time rank. ***F***, A grand average seizure recruitment rank heatmap, taken across all individual mouse average maps after co-registration. ***G***, A grand average seizure peak ΔF/F rank heatmap, taken across individual mouse averages. ***H***, A grand average heatmap of ranked seizure duration at each pixel, taken across individual mouse averages.

in our IED analysis, we then grouped events with similar spatial profiles using hierarchical clustering. To quantify the spatial profile of each cluster, we calculated the average peak intensity in each cortical area across all events in the cluster, first within individual mice and then within *Kcnt1*$^{m/m}$ and WT groups (Fig. 5, line plots). Additionally, we generated average event peak intensity images for each cluster and genotype (Fig. 5, images).

Two features of these data indicate that clusters represent event types that occur commonly, and are equivalent, in both WT and *Kcnt1*$^{m/m}$ mice. First, although events from both groups were first pooled and clustered without respect to genotype, each cluster contained many events from both WT and *Kcnt1*$^{m/m}$ mice (Fig. 5, line plot text insets). If the spatial organization of events in *Kcnt1*$^{m/m}$ mice differed significantly, and systematically, from WT, we would expect clusters comprised mainly of one genotype or the other. Second, events from both genotypes in a cluster showed similar spatial profiles, as evidenced by their average peak intensity images and the high positive correlation coefficient between the peak intensity traces (significant at 0.005 for all clusters, median = 0.97, std = 0.05). This does not mean events in the same cluster were identical in WT and *Kcnt1*$^{m/m}$ mice; some clusters showed variation in average intensity in some cortical areas. However, even in these cases, the spatial distribution of activity was highly correlated across groups. Thus, the major types of cortical activity observed in WT mice were preserved in *Kcnt1*$^{m/m}$ mice, and there was no evidence of novel event types in *Kcnt1*$^{m/m}$ mice during interictal cortical activity. These data suggest that large scale disruption of cortical arealization and connectivity are not necessary to support frequent spontaneous seizures and IEDs and, conversely, that seizures and IEDs do not necessarily cause such disruptions.

Long-range seizure propagation follows normal corticocortical synaptic connections

The lack of novel event types in *Kcnt1*$^{m/m}$ mice suggests that connections between cortical areas are grossly normal. However, seizures have the potential to re-wire the neural circuits in which they occur, and the correspondence between cortical subnetworks engaged by interictal and epileptic activity is unclear. To investigate whether seizure activity, like interictal activity, also occurs within a cortical network common to both *Kcnt1*$^{m/m}$ and normal mice, we identified instances when seizures made long-range jumps to tissue that was noncontiguous with the emergence zone (Fig. 6*A–C*). We then tested whether these jumps occurred between areas that were synaptically connected in normal mice and, if so, how strongly, by comparing them to a previously published model of corticocortical connectivity based on the Allen Connectivity Atlas (Fig. 6*D*; Oh et al., 2014). We found that areas between which seizures jumped had a 0.86 connection probability, which was higher than any observed after randomly repositioning primary and secondary seizure locations (10,000 repetitions; Fig. 6*E*). Likewise, connection strength between areas

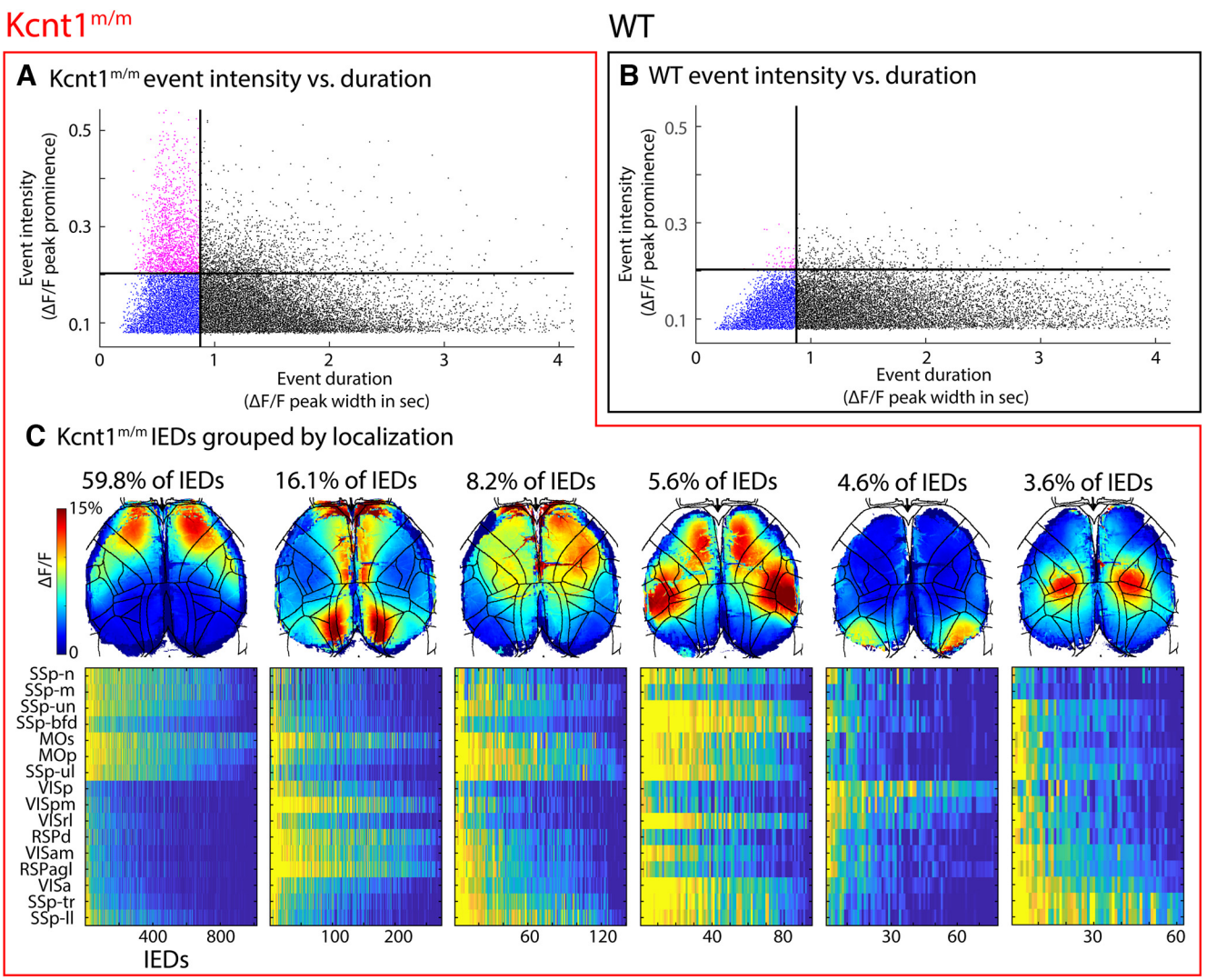

Figure 3. Mapping IEDs reveals partial overlap with seizure susceptible regions. ***A***, ***B***, Scatter plots of event intensity versus duration for events detected in *Kcnt1*$^{m/m}$ (***A***) and WT (***B***) mice. Event intensity was measured as the 99th percentile of ΔF/F peak prominences on all event pixels and duration was measured as the mean with at half peak prominence calculated over all event pixels. Horizontal lines mark IED intensity threshold (0.20), and vertical lines mark IED duration threshold (0.875 s). Plots were cropped to highlight region relevant to IED detection. ***C***, Images show the average ΔF/F frame taken across all the IEDs within clusters produced by hierarchical clustering. The value of pixels outside the IED were set to zero in frames contributing to these averages. Above each image, the percentage of all *Kcnt1*$^{m/m}$ IEDs contained in the cluster is given. Three small clusters collectively representing 1.9% of IEDs are not shown. Below, Individual heatmaps show average ΔF/F in each cortical area for all IEDs in the cluster. Color bar applies to images and heatmaps. See Clustering section for discussion of cluster number selection.

that spanned a jump was 0.39, a value greater than any observed after randomly re-drawing strengths (10,000 repetitions; Fig. 6*F*), likely because true primary-to-secondary seizure area pairs contains far fewer weak connections than the model at large. These analyses showed that seizure activity jumps between synaptically connected cortical areas at much greater than chance frequency and that the connections are, on average, unusually strong. This argues that seizure activity, like interictal activity, in these chronically epileptic brains is supported by grossly normal patterns of corticocortical synaptic connectivity.

However, connection strength was not the sole determinant of seizure propagation patterns. For example, the model predicts that primary visual cortex (VISp) receives strong input from the area most likely to host seizure emergence (PTLp), yet it was remarkably resistant to *Kcnt1*$^{m/m}$ seizures (Figs. 2, 3*C*,*D*). Additionally, *Kcnt1*$^{m/m}$ seizures that began in MOs jumped most often to PTLp, although several other regions in our FOV are predicted to receive stronger inputs from this area (Fig. 6*C*,*D*). Thus, seizures seem to propagate along normal synaptic connections with a bias toward downstream areas that show features of seizure susceptibility beyond early recruitment (i.e., host emergence, intense and prolonged seizure involvement).

Seizures emerge from cortical activity patterns that also occur during the interictal period

Our results, thus far, indicate that the mesoscale structure of cortical networks supporting interictal activity in *Kcnt1*$^{m/m}$ mice is largely normal and that seizures use these networks for long-range propagation. However, they do not address whether these normal networks also support seizure generation or are simply coopted after a seizure has begun. Given the importance of seizure initiation as a therapeutic target, characterizing the network involved in seizure onset and early growth is critical. We thus asked the question of whether activity patterns immediately preceding seizures were unique to this period. To accomplish this, we first identified cortical events that immediately preceded seizures, which largely showed peak activity concentrated in the impending emergence zone (Fig. 7*A*). We then compared the

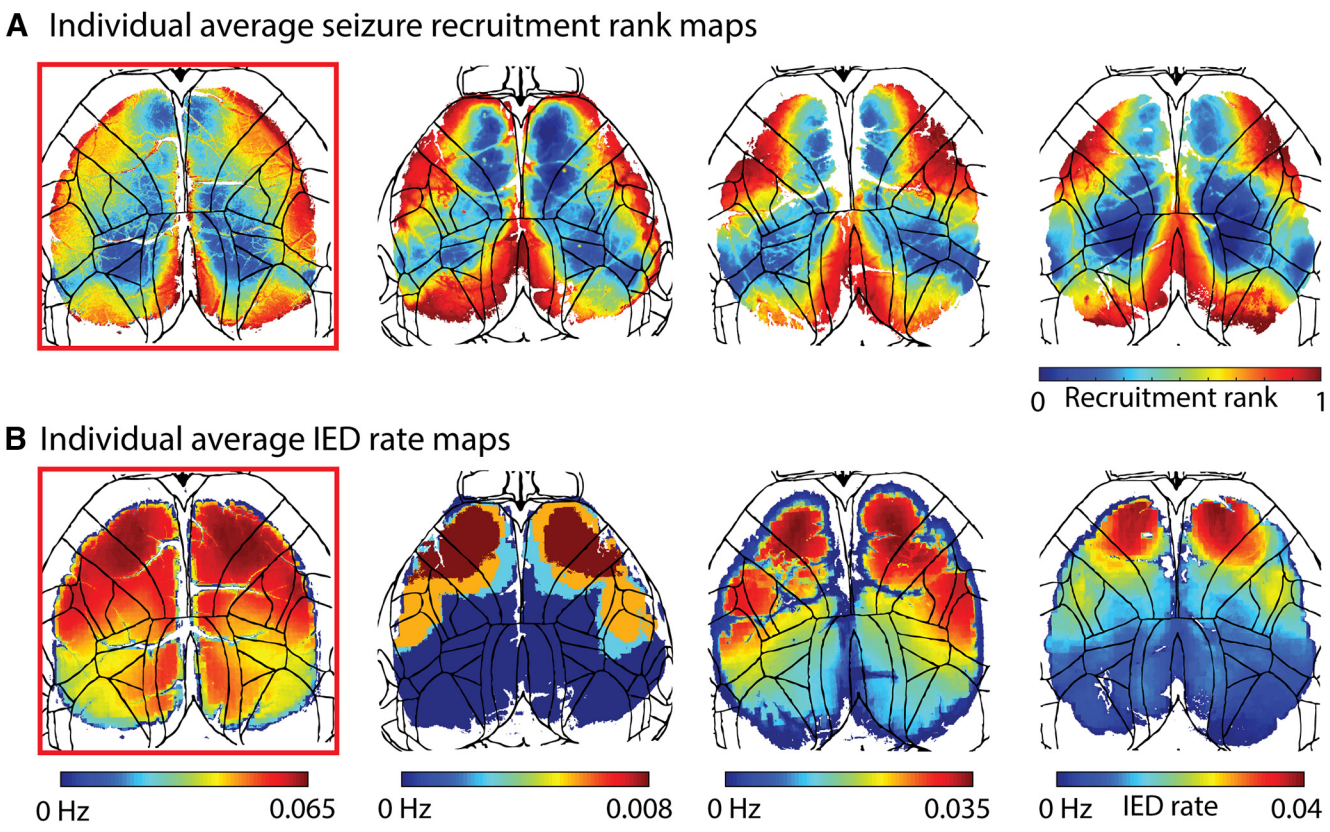

Figure 4. Comparison of seizure recruitment and IED maps in individual *Kcnt1*$^{m/m}$ mice. ***A***, Average seizure recruitment rank heatmaps for each *Kcnt1*$^{m/m}$ mouse that experienced seizures during imaging. The value of each pixel is its recruitment time rank. ***B***, Average IED rate map for each animal in ***A***. The value of each pixel is the average rate of IEDs taken over all sessions where event detection was performed. Red boxes identify data from the mouse that was implanted with a glass cranial window.

peak activity (top 5% ΔF/F) of these preseizure events to those of all interictal events in the dataset and gave each event a match score (0–1; see Experimental methods). Interictal events were divided into three groups: events from the animal that produced the preseizure pattern (source mouse), other *Kcnt1*$^{m/m}$ mice, and WT mice (Fig. 7*B*), to determine whether preseizure activity patterns were unique to any of these categories. To quantify the overall degree of similarity, we used the same matching approach to measure how similar interictal events of the same cluster (Fig. 5) were to each other and generated a null distribution of match scores. This showed that the highest match scores of preseizure patterns to interictal events typically fell within the null distribution 95% CI across all groups (Fig. 7*C*), indicating that the difference between preseizure and normal interictal patterns is no greater than between the most similar interictal events, and that event types similar to preseizure events are found even in WT mice. Top match scores for a few preseizure patterns fell below the 95% CI, likely because of the fact that preseizure patterns came from the last frame before seizure onset, when activity was typically already elevated across much of the FOV. This analysis demonstrates that most seizures emerge from cortical activity patterns that also occur interictally, supporting the hypothesis that normal cortical networks support seizure generation.

Abnormally persistent activity in the seizure emergence zone precedes seizure onset

The finding that the spatial profile of cortical activity is not abnormal leading up to seizure led us to search for alternative features of activity that may distinguish the preseizure phase. In analyzing calcium imaging frames just before individual seizures, we observed that preseizure activity patterns appeared to repeat many times and persist for prolonged periods in the lead up to seizure. Because preseizure events encompass emergence zones, this suggests that a progressively larger fraction of cortical activity in the preseizure period localizes to the future site of seizure emergence. To assess this more quantitatively, we calculated the match score between each preseizure event and every other frame collected during the 20 s before seizure onset (Fig. 7*D*). This analysis showed that the lead up to seizure was characterized by a ramping increase in the match score (Fig. 7*D*,*F*, heavy black line). To determine whether this increase was a statistically significant result, we calculated match scores in the lead up to interictal occurrences of events similar to the preseizure pattern (see Preseizure image template matching; Fig. 7*E*), and created a null distribution using the top 50 matches (Fig. 7*F*, magenta lines.) A comparison of preseizure match scores to the null distribution showed that, starting 9.4 s before seizure onset, cortical activity is significantly more concentrated in the impending seizure emergence zone than would be expected in the lead up to a similar activity pattern outside of seizures and IEDs (Fig. 7*F*). This is true even before the preseizure peak activity level exceeds that of interictal frame matches (period between −9.4 and −2.4 s; Fig. 7*G*). Thus, while the mesoscale spatial pattern of activity in the preperiod is not abnormal, its temporal dynamics are, and importantly, these data further indicate that a persistent concentration of activity in the impending emergence zone predicts seizure onset.

Excessive interictal activity predicts epileptic vulnerability among cortical areas

The above data indicate that epileptic activity occurs within the same cortical networks that support interictal activity in both

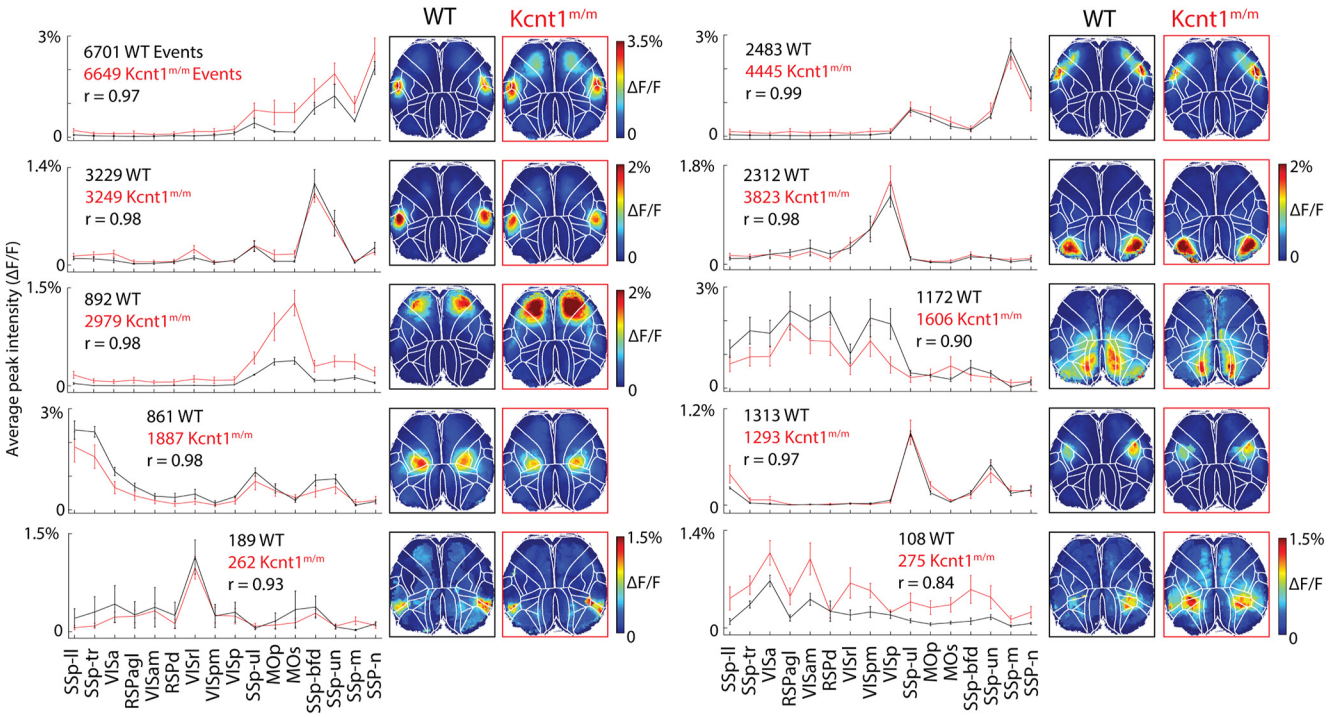

Figure 5. Mesoscale interictal activity is comprised of event types with equivalent spatial structure in *Kcnt1*$^{m/m}$ and WT mice. Line plots show the average peak intensity of neural activity within each Allen Mouse CCF area imaged. These values were constructed by taking the average ΔF/F peak value across all pixels involved in an event in each area. Pixels not involved in the event were set to zero. Lines represent grand averages for each group, taken across session averages for each mouse. Error bars show SEM across mouse averages. Text above each plot gives the total number of events in the cluster from each group and the *Kcnt1*$^{m/m}$ to WT Pearsons correlation coefficient. Images to the right of each line plot show the average event peak intensity at all pixels for each genotype and cluster. These were calculated using event frames in which each pixel was assigned its ΔF/F peak intensity value, and pixels not involved in the event were set to zero. The color bar in the top left applies to all images in the figure except for those where another color bar is present.

Kcnt1$^{m/m}$ and WT mice, but that the magnitude and dynamics of this activity may be altered in such a way as to predispose it to seizures. To more systematically measure how these features of interictal activity in the *Kcnt1*$^{m/m}$ brain differ from WT, we calculated the rate and duration for each interictal event type in both groups (Fig. 5). Because the number of sessions per animal differed, *Kcnt1*$^{m/m}$ and WT group averages were weighted by the number of sessions from each mouse. Figure 8*A* shows an example of this approach in measuring rate in the cluster with peak activity in the PEZ.

The rate of events was significantly altered in five of the 10 event types (Fig. 8*B*). Four showed increased rates in *Kcnt1*$^{m/m}$ mice, and one decreased, relative to those of WT. Notably, each event type with an elevated rate in *Kcnt1*$^{m/m}$ mice showed peak activity in cortical areas susceptible to seizures and IEDs (Fig. 8*B*). The cluster that showed a decrease localized to SSp-ul, an area not notably susceptible to seizures or IEDs (Fig. 8*B*). These results indicate that a distinguishing feature of tissue prone to epileptic pathology is the presence of excessively frequent events during interictal periods.

Event duration was reduced in five of the 10 event types and increased in none (Fig. 8*C*). Three of five event types were the same ones that showed increased rate and involved seizure and IED susceptible areas. The largest duration reduction was in the event type centered on MOs, and the next two largest were also in event types centered on vulnerable areas (Fig. 8*C*, asterisks). Events centered on the PEZ, the most common seizure emergence zone, showed a decrease in duration that failed to achieve statistical significance; however, statistical power was limited by the low rate of occurrence of these events in WT mice coupled with the relatively large number of events we needed to attain a stable duration estimate ($n = 15$; see Materials and Methods). We also found smaller, but significant, reductions among events with peak activity in VISp and SSp-ul, seizure resistant areas in which rate was unchanged and decreased in *Kcnt1*$^{m/m}$ mice, respectively. Thus, event duration was reduced in several cortical areas, especially those that were seizure susceptible.

The intensity of cortical events across clusters predicts epileptic activity burden

We analyzed event intensity in the same manner as rate and duration and found that only the cluster including MOs was significantly higher, whereas none were significantly lower. However, inspection of the data showed that the most striking feature of intensity was its variability in *Kcnt1*$^{m/m}$ mice, regardless of event cluster. Although WT mice showed relatively consistent intensity values across individuals and sessions, *Kcnt1*$^{m/m}$ mice had high individual variability in event intensities; some individuals showed characteristically lower intensity than WT, and others higher (Fig. 9*A*). This effect was consistent across sessions from the same mouse and was most evident in the grand average intensity taken across event types, indicating that it was a global effect distributed throughout the cortex. This variation in event intensity among mutant mice suggests the YH variant can produce divergent outcomes in different individuals, and led us to investigate how global intensity of cortical activity relates to the occurrence of epileptic activity.

To quantitatively compare global event intensity and epileptic activity burden in individual mice, we first created a matrix containing median peak intensity for each event type (Fig. 9*B*, columns) by mouse (rows). We then estimated each mouse's global intensity scaling factor by performing SVD. The resulting first

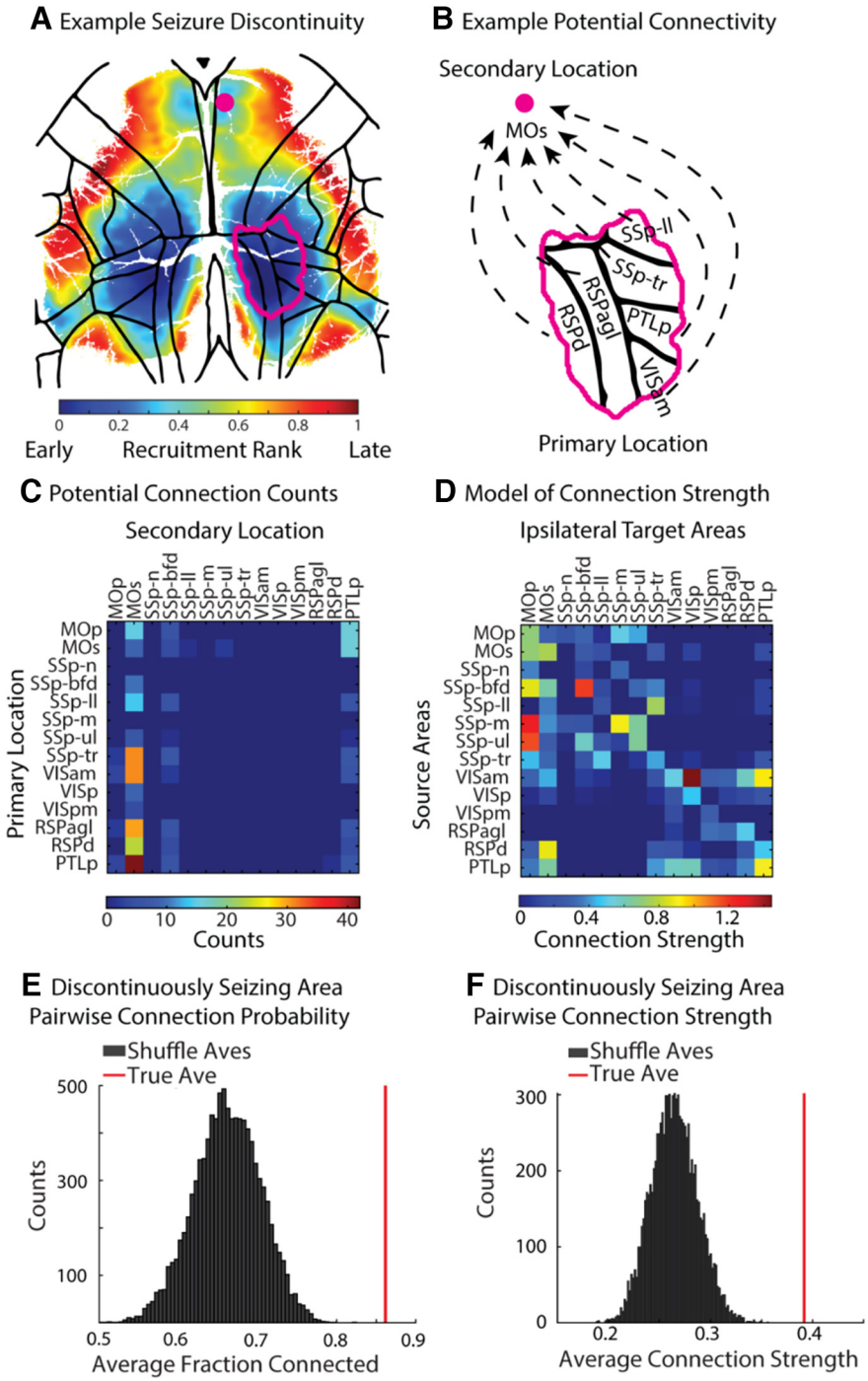

Figure 6. Long-range seizure propagation follows normal corticocortical synaptic connections. ***A***, An example seizure rank recruitment heatmap showing a long-range jump in seizure propagation. The magenta border indicates the extent of seizing tissue in the primary location at the time the seizure emerged at the secondary location, marked by a magenta dot in MOs. ***B***, A diagram indicating synaptic connections potentially mediating propagation between each of the areas in the primary and secondary seizure locations. ***C***, A heat-map indicating the number of times each pair of cortical areas was found in primary and secondary seizure locations following a long-range jump. ***D***, A heatmap showing area-to-area connection strength in the interarea connectivity model adapted from Oh et al. (2014), cropped to include only areas in our FOV. ***E***, Results of a simulation to test primary to secondary area connection probability against a random draw from the model in ***D***. Simulated averages are shown by the histogram and the true average by the red line. ***F***, Results of a shuffle analysis to compare the connection strength between primary and secondary seizure locations to a random draw from the connectivity model in ***D***. Histogram shows simulated averages, and the red line marks the true average connection weight.

singular vectors and value model the matrix as a common intensity-by-event-type curve (Fig. 9*B1*) multiplied by a global intensity scaling factor for each individual (Fig. 9*B2*). This step was necessary to ensure that the increase in the average intensity was truly global and not driven by a few high intensity events or clusters. We next quantified epileptic activity burden for each *Kcnt1*$^{m/m}$ mouse by averaging the normalized total seizure time and average IED rate for each mouse, and then plotted epileptic activity burden as a function of global intensity scaling (Fig. 9*C*). This revealed a strong, positive correlation, mice with high intensity scaling factors suffered high epileptic activity burdens, while those with small scaling factors suffered less. The shape of the relationship between epileptic activity burden and intensity scaling factor was sigmoidal and well fit by a logistic function (Fig. 9*C1*). We then plotted a hypothetical epileptic activity burden for WT mice based on their global intensity scale factor and the fit calculated from *Kcnt1*$^{m/m}$ mice. Comparing these hypothetical values to actual values from *Kcnt1*$^{m/m}$ mice on the curve showed that the two *Kcnt1*$^{m/m}$ mice in which no seizures were observed and had the lowest IED rates had event intensities below any WT mouse (Fig. 9*C2*). This indicates that the global intensity of cortical activity needs to be scaled well below WT levels to prevent the occurrence of epileptic activity.

These data reveal a strong relationship between disease burden and a specific feature of interictal cortical activity, its peak intensity. It is interesting that variation in event intensity was not mirrored by similar variation in event rate at the level of individual mice. Thus, YH-driven cortical hyperactivity manifests in several distinct forms, subject to independent modulation, and showing specific, yet distinct, relationships to epileptic pathology. While elevated event rates predicted the localization of seizures and IEDs, the characteristic intensity of an individual's cortical intensity predicted its disease burden.

Discussion

The chronically epileptic network in *Kcnt1*$^{m/m}$ mice coopts the existing mesoscale cortical network

Comparing *Kcnt1*$^{m/m}$ with WT mouse cortical activity via widefield calcium imaging suggests that KCNT1-related seizures operate within the constraints of a normal mesoscale network and do not result in the formation of novel networks during epileptogenesis (Beenhakker and

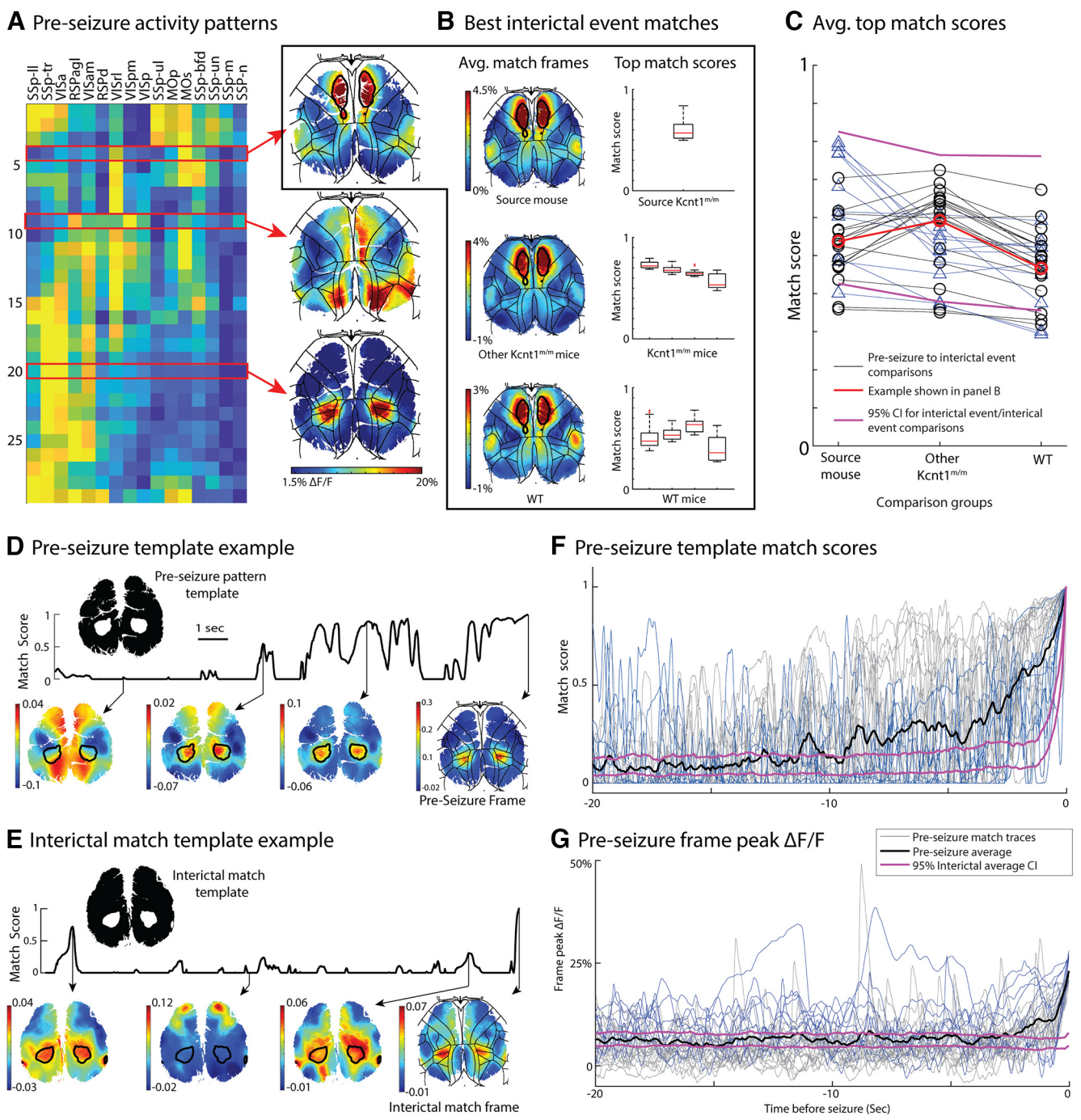

Figure 7. Abnormally persistent activity in the seizure emergence zone precedes seizure onset. ***A***, Heatmap showing Allen Mouse CCF area scaled average ΔF/F values in the last frame before seizure emergence, ordered according to optimal leaf order after hierarchical clustering. At right are two example preseizure patterns with CCF area boundaries overlaid. The top image shows boundaries of the preseizure peak activity (black outline). ***B***, Average images and match score distributions for the best interictal event matches from the source mouse (top), other *Kcnt1*$^{m/m}$ mice (middle), and WT mice (bottom) to the uppermost example preseizure activity pattern in ***A***. ***C***, Summary data of the average top match scores for each preseizure activity pattern (black lines indicate mice imaged through an intact skull, blue lines, indicate data from the mouse with a glass cranial window) compared with all interictal events from the source mouse, other *Kcnt1*$^{m/m}$, and WT mice. Magenta lines show 95% confidence interval (CI) of the null distribution. ***D***, An example preseizure template match score trace in the 20 s lead up to seizure onset with representative frames, with template boundaries overlaid, shown below. ***E***, An example interictal template match score trace in the lead up to a top 50 interictal frame match to the preseizure activity pattern shown in panel ***D***. ***F***, A comparison of template match scores in the 20 s lead up to seizures, and interictal match frames. Gray traces show individual preseizure template match scores, and the black trace shows the average across all preseizure traces. Magenta lines show the 95% CI for a match score average calculated over a random selection of top 50 interictal match frames for each preseizure template. Blue lines indicate data from the mouse implanted with a glass cranial window. ***G***, A comparison of frame peak ΔF/F in the lead up to seizures, and interictal match frames. Gray traces show frame peak ΔF/F in the lead up to each seizure, and the black trace is the average across all preseizure traces. Magenta lines show the 95% CI for a frame peak ΔF/F average calculated over a random selection from the top 50 interictal matches to each preseizure template. Blue lines indicate data from the mouse implanted with a glass cranial window.

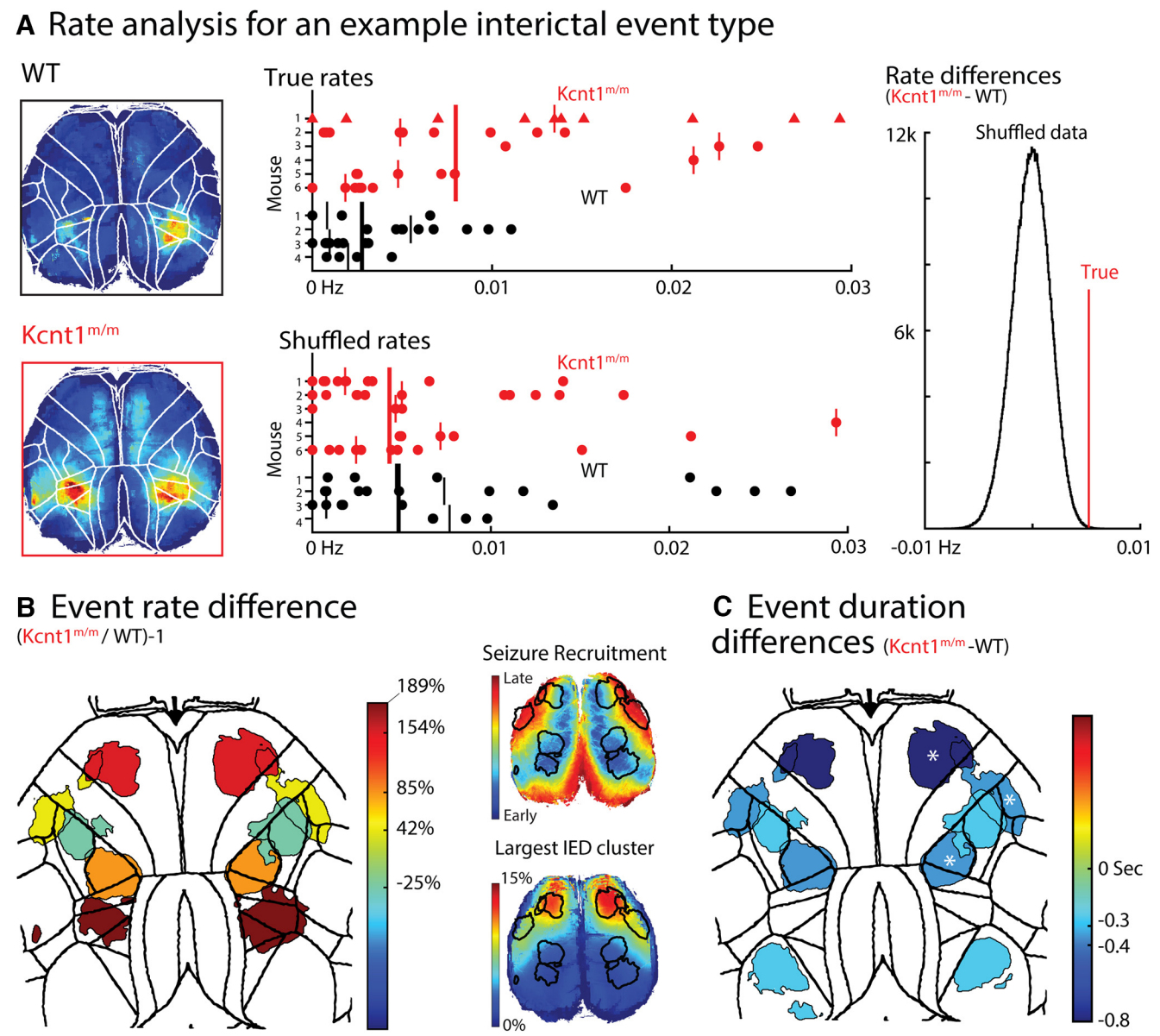

Figure 8. Excessive interictal activity predicts epileptic vulnerability of cortical areas. ***A***, Illustration of the approach to measuring interictal event rate differences between genotypes for an example event type. Event peak intensity images from WT and *Kcnt1*$^{m/m}$ mice are shown on the left. The upper scatter plot shows event rates of all sessions in each mouse. Each row on the *y-axis* represents all session from one mouse and each dot represents the mean event rate from one imaging session. Lower plot shows the same data after a random shuffle in which the event rate, calculated in each session from each mouse, was pooled, shuffled, and then redrawn such that each mouse had the same number of sessions before and after the shuffle. Short lines are animal medians and long lines are group means weighted by session number. Histogram to the right shows the distribution of weighted group average differences obtained from 1 million shuffles, the red line indicates the true group difference (>99.96% of shuffled group differences). ***B***, Heatmap on the left indicates clusters in which event rate is significantly different in *Kcnt1*$^{m/m}$ mice (permutation test, $p < 0.05$ Bonferroni–Holm corrected). Patch color indicates the fractional change in event rate and the borders demarcate peak activity in the cluster event mean image. To highlight the correspondence between seizure and IED susceptibility and increased rate of interictal activity, the grand average seizure recruitment rank map (Fig. 2*F*) and the average image for the largest IED cluster (Fig. 5*C*) are shown with the peak activity borders for clusters with increased event rates in *Kcnt1*$^{m/m}$ mice overlaid. ***C***, Heatmap indicating clusters in which event duration, measured as event width-at-half-max, is significantly decreased in *Kcnt1*$^{m/m}$ mice (permutation test, $p < 0.05$ Bonferroni–Holm corrected). Patch color indicates the absolute change in event duration and the borders demarcate peak activity in the cluster event mean image. Asterisks indicate seizure or IED susceptible regions. Data from the mouse implanted with a glass cranial window is marked by red triangles.

Huguenard, 2009; Kramer and Cash, 2012; Smith and Schevon, 2016; Zaveri et al., 2020). First, the spatial profile of interictal events was similar between *Kcnt1*$^{m/m}$ and WT mice (Fig. 5), suggesting that, interictally at least, there are not functional, *de novo*, long-range connections in the chronically epileptic *Kcnt1*$^{m/m}$ brain. Our analyses do not rule out increases in local hyperconnectivity, however, of which there is clear evidence for in the literature in several epilepsy models (Lynch and Sutula, 2000; Scharfman et al., 2003; Shao and Dudek, 2004; Chu et al., 2010; Barrows et al., 2017), including the *Kcnt1* model (Shore et al., 2020). Second, most seizures arose out of activity patterns that also occurred during the interictal period (Fig. 7), suggesting that, even immediately before seizure, when the overall intensity of cortical activity is high, the cortex still respects the spatial boundaries of normal brain activity. Finally, long-range seizure propagation preferentially occurred along synaptic connections found in the normal brain (Fig. 6). These findings in our genetic model are consistent with recent studies of chemically and

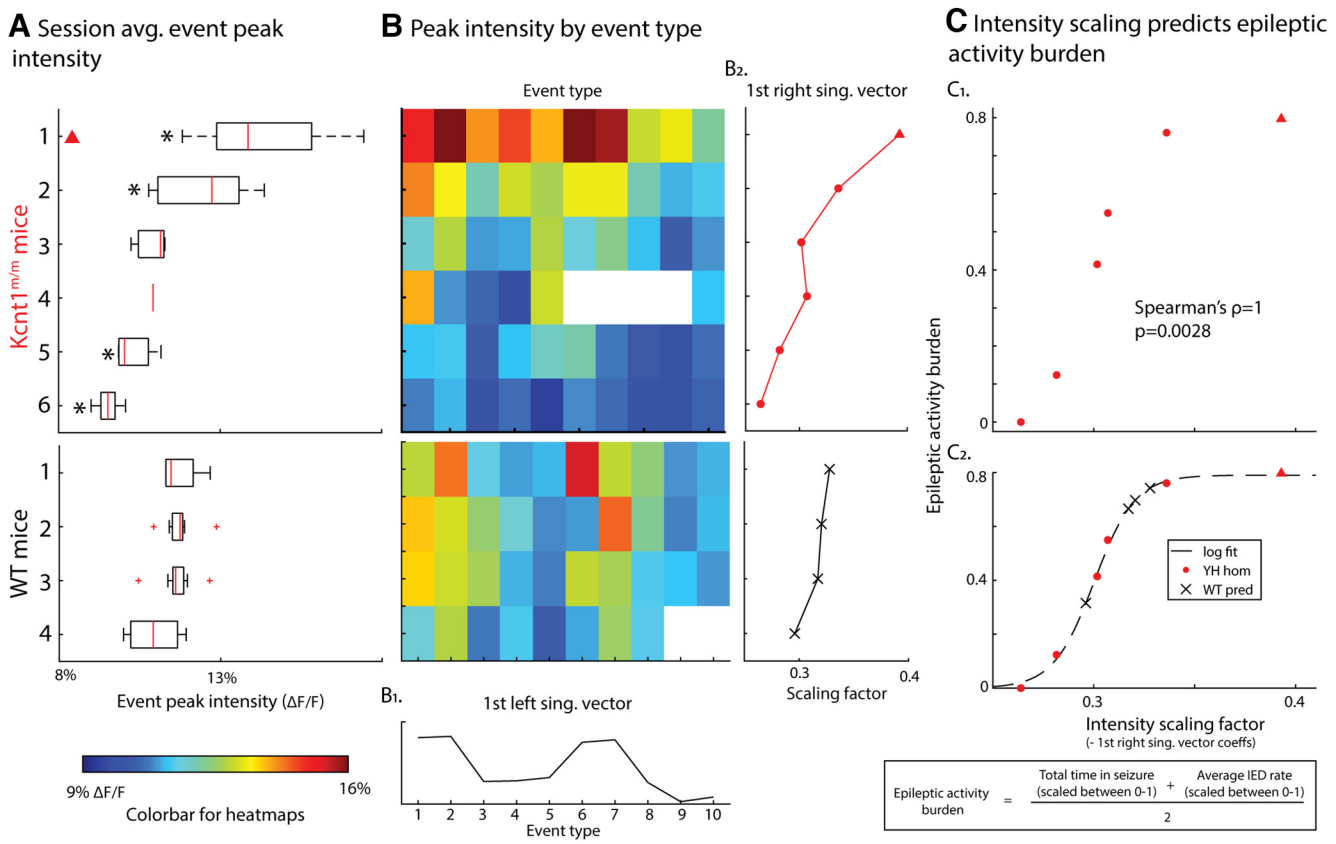

Figure 9. Global scaling of cortical event intensity predicts epileptic activity burden. ***A***, Boxplots of session average event peak intensities for all sessions in which event detection was performed in each mouse, numbered as in Figure 8. Asterisks mark *Kcnt1*$^{m/m}$ mice that differed significantly from the WT distribution (permutation test, $p < 0.05$). ***B***, Heatmap showing event peak intensity for each event type in each mouse. Values are medians taken over session averages mapped by the color bar in the lower left of the figure. Mouse identify from panel ***A*** is preserved along rows. Performing SVD on this matrix yields a first left singular vector (***B*$_1$**) representing the pattern of intensity variation across event types, and a first right singular vector (***B*$_2$**) representing how this pattern is scaled in each individual. ***C***, Epileptic activity burden plotted as a function of individual event intensity scaling factors (right singular vector values from ***B*$_1$**). ***C*$_1$** shows values for *Kcnt1*$^{m/m}$ mice (red dots), their Spearman's correlation coefficient, and associated *p* value. ***C*$_2$** shows a logistic fit to *Kcnt1*$^{m/m}$ data $y = 0.79/(1+e^{a}(-98.9(x - 0.3)))$, and hypothetical WT epileptic activity burdens predicted by this fit. Data from the mouse implanted with a glass cranial window is marked by red triangles.

optogenetically induced seizures in WT mice (Rossi et al., 2017; Choy et al., 2022). Additionally, our finding that long-range seizure propagation was biased toward synaptically downstream areas that are, themselves, seizure susceptible, is similar to previous findings that long-range seizure jumps occur preferentially to distant, pharmacologically disinhibited areas (Liou et al., 2018). This parallel suggests that seizure susceptibility in *Kcnt1*$^{m/m}$ mice may coincide with where inhibition is most severely compromised, which we previously showed was a direct effect of the *Kcnt1* YH variant (Shore et al., 2020). Future studies that compare the cellular, circuit, or genetic factors that make some areas vulnerable, and others resistant to, seizures in this model and others will be valuable.

We cannot rule out the possibility that our approach is not sensitive enough to detect the formation of novel networks or event types in the *Kcnt1*$^{m/m}$ brain that mediate epileptogenesis, or that we have failed to identify the true site of seizure initiation. The method we used to identify interictal event types yielded broad categories of spatial activity patterns at a resolution constrained by the Allen CCF cortical area map. Novel event types that occur infrequently or differ in the fine details of their spatial profile could be missed. Furthermore, the Y796H mouse models a sleep-associated epilepsy, and we did not monitor sleep state in this study. Our observations of these mice lead us to believe that they rarely sleep during imaging sessions, thus, we may have missed abnormal brain activity that is associated with nonrapid eye movement (NREM) sleep.

A limitation of widefield imaging is that, although we monitored a large fraction of the cortex, we were unable to monitor activity in the entire brain, including several subcortical structures known to play important roles in seizure generation. Although it is almost certain that areas outside our FOV are playing a role, and we may have not captured the generative network, several aspects of our data are inconsistent with exclusively remote seizure and IED initiation. Our core finding of excessive interictal activity in susceptible areas argues that they are at least a portion of the generative network. Such correlations in space and time between interictal abnormalities and epileptiform activity are hard to reconcile with a purely remote seizure and IED origin. For example, abnormally persistent activity in the seizure emergence zone begins over 9 s before seizure onset and becomes more pronounced as seizure approaches. During this period, we are unable to see any behavioral indication of seizure, although these signs commence simultaneously with cortical seizure onset.

A single gene variant in an inbred mouse strain has diverse effects on interictal neural activity

One of the most surprising findings of our study is the diversity of effects on cortical activity caused by a single gene variant. This variation manifests itself at the level of both cortical area and

individual mice, and has implications for basic and preclinical research. For instance, despite widespread expression of KCNT1 in the cortex (Bhattacharjee et al., 2002; Martinez-Espinosa et al., 2015; Rizzi et al., 2016), the variant caused excessive interictal activity in some areas, but reduced activity or altered temporal dynamics in others. First, the fact that the variant had opposite effects on neural activity in different cortical areas speaks to the importance of localizing pathology in animal models before performing targeted experiments such as patch clamp electrophysiology or gene expression studies. If the effect of a genetic change is not known a priori, as in the majority of genetic mouse models carrying human disease-causing variants, then studying an area that shows reduced activity and is seizure resistant will likely lead to different experimental results than studying an area with increased activity that is seizure-vulnerable (Rakhade et al., 2007; Kullmann et al., 2012; Debanne et al., 2019). Comparing such areas could lead to better understanding of the factors underlying region susceptibility and robustness to epileptic activity. Previously, we showed that nonfast spiking interneurons neurons from M2 showed strong reductions in membrane excitability in this model. Thus, future experiments testing whether this neuron type is also affected in other seizure susceptible areas (PTLp) and seizure resistant areas (S1) could answer the question of whether certain cell types or circuit architectures confer regional susceptibility.

Second, the observation that the same variant caused opposite effects in different cortical regions, which are comprised of broadly similar cell types and circuits (Harris and Shepherd, 2015), suggests that the altered brain functions that subserve epileptic pathology are several steps removed from the cellular roles of the molecules that underly them. One explanation for this is that we imaged adult mice, well after the onset of epilepsy in this model. Future studies performing longitudinal imaging throughout key developmental timepoints (Domínguez et al., 2021) could inform whether the rate and intensity changes that we observed evolve through development, and how these developmental alterations might relate to the ultimate expression of overt pathology. Furthermore, our results showing qualitatively different effects on activity in different cortical areas strongly argues that interventions targeted to specific brain areas are needed to maximize treatment and minimize side effects, even when the therapy is gene-based (Epi, 2015; Turner et al., 2021). For instance, therapies designed to broadly restrict excitability may reduce seizures and IEDs by bringing the activity of some regions into a normal range, but may simultaneously reduce the activity of other regions below key thresholds, thus, risking collateral disruption of brain functions uninvolved in disease.

Excess frequency of events identifies seizure susceptible cortical regions

Despite the diversity of effects of the variant in different cortical areas, a logic to the changes emerged when we compared them to the areas that were vulnerable to seizures and IEDs, suggesting cortical area is a strong determinant of pathologic outcome. The variant predictably drove epileptic activity, and excessive interictal activity, in a restricted subset of areas. Elsewhere, it reduced activity and altered its temporal dynamics without generating seizures and IEDs. Previous studies have indicated that epileptic tissue is hyperexcitable (Valentín et al., 2002; Polack et al., 2007; Brigo et al., 2013; Williams et al., 2016), thus, it is not surprising that areas vulnerable to seizure and IED show activity profiles that suggest underlying hyperexcitable circuits, such as increased event rate or intensity. A more salient question then, is whether area-specific increases in interictal activity cause seizures, are a consequence, or both arise from the same underlying circuit change. Although this is a difficult question to answer definitively, the fact that *Kcnt1*$^{m/m}$ animals that showed few or no seizures still showed elevated rate and intensity in seizure-prone areas suggests that elevated interictal activity is not a consequence of seizures.

Global intensity scaling in individuals suggest compensatory plasticity can protect against epilepsy

The finding that some *Kcnt1*$^{m/m}$ mice had no observed seizures and reduced intensity, whereas others had many seizures and increased intensity, suggests that seizure burden is proportional to the global intensity of interictal cortical activity, at least in this model. That some mice had lower than WT intensity suggests that seizures themselves are not the cause of intensity differences, but that there is a mechanistic link between altered intensity and the seizure burden. Thus, the lowering of intensity may be a homeostatic response to compensate for the proexcitatory effect of the variant and prevent seizures, while the raised intensity may reflect a failure of this mechanism.

The cortex-wide nature of this scaling is surprising, as is the large variation in individual *Kcnt1*$^{m/m}$ mice. In humans, genotype/phenotype correlations from the same variant are often poor, an observation that has been attributed to background genetic variation or experience (Helbig and Tayoun, 2016). Our mice, however, are all highly genetically similar and housed in similar conditions. Some were littermates. This suggests an unappreciated stochasticity in the development of mesoscale activity in the epileptic brain. Alternatively, a period of reduced cortical activity may be a disease stage that occurs in all mutant mice. However, because we followed most individual mice over a period of weeks at roughly the same age, during which time cortical activity levels were stable, this interpretation requires a high degree of interindividual variability in disease progression. In either case, these results suggest that, although it may protect from seizures, compensatory intensity downscaling comes at the cost of pushing some features of interictal activity further away from WT levels.

These findings have direct implications for the development of precision epilepsy therapies. The large variation between *Kcnt1*$^{m/m}$ mice suggest that even individuals with the same disease-causing genetic variant may need to be treated differently, depending on their disease progression. We provide a clear roadmap for measuring how severely brain activity deviates from normal, not only in pathologically active areas, but across large portions of the brain and outside of epileptic activity. This information can potentially be used to determine where and how brain activity needs to be modulated to holistically restore normal function. It also has the potential to reveal unintended off-target treatment effects, facilitating therapy optimization to deliver maximal benefit with minimal side-effect potential.

References

Allen WE, Kauvar IV, Chen MZ, Richman EB, Yang SJ, Chan K, Gradinaru V, Deverman BE, Luo L, Deisseroth K (2017) Global representations of goal-directed behavior in distinct cell types of mouse neocortex. Neuron 94:891–907.e6.

Baird-Daniel E, Daniel AGS, Wenzel M, Li D, Liou JY, Laffont P, Zhao M, Yuste R, Ma H, Schwartz TH (2017) Glial calcium waves are triggered by seizure activity and not essential for initiating ictal onset or neurovascular coupling. Cereb Cortex 27:3318–3330.

Barcia G, et al. (2019) Epilepsy with migrating focal seizures: KCNT1 mutation hotspots and phenotype variability. Neurol Genet 5:e363.

Barrows CM, McCabe MP, Chen H, Swann JW, Weston MC (2017) PTEN loss increases the connectivity of fast synaptic motifs and functional connectivity in a developing hippocampal network. J Neurosci 37:8595–8611.

Beenhakker MP, Huguenard JR (2009) Neurons that fire together also conspire together: is normal sleep circuitry hijacked to generate epilepsy? Neuron 62:612–632.

Bhattacharjee A, Gan L, Kaczmarek LK (2002) Localization of the Slack potassium channel in the rat central nervous system. J Comp Neurol 454:241–254.

Brigo F, Bongiovanni LG, Nardone R, Trinka E, Tezzon F, Fiaschi A, Manganotti P (2013) Visual cortex hyperexcitability in idiopathic generalized epilepsies with photosensitivity: a TMS pilot study. Epilepsy Behav 27:301–306.

Budelli G, Hage TA, Wei A, Rojas P, Jong YJ, O'Malley K, Salkoff L (2009) Na+-activated K+ channels express a large delayed outward current in neurons during normal physiology. Nat Neurosci 12:745–750.

Choy M, Dadgar-Kiani E, Cron GO, Duffy BA, Schmid F, Edelman BJ, Asaad M, Chan RW, Vahdat S, Lee JH (2022) Repeated hippocampal seizures lead to brain-wide reorganization of circuits and seizure propagation pathways. Neuron 110:221–236.e4.

Chu Y, Jin X, Parada I, Pesic A, Stevens B, Barres B, Prince DA (2010) Enhanced synaptic connectivity and epilepsy in C1q knockout mice. Proc Natl Acad Sci U S A 107:7975–7980.

Daniel AG, Laffont P, Zhao M, Ma H, Schwartz TH (2015) Optical electrocorticogram (OECoG) using wide-field calcium imaging reveals the divergence of neuronal and glial activity during acute rodent seizures. Epilepsy Behav 49:61–65.

Debanne D, Inglebert Y, Russier M (2019) Plasticity of intrinsic neuronal excitability. Curr Opin Neurobiol 54:73–82.

Domínguez S, Ma L, Yu H, Pouchelon G, Mayer C, Spyropoulos GD, Cea C, Buzsáki G, Fishell G, Khodagholy D, Gelinas JN (2021) A transient postnatal quiescent period precedes emergence of mature cortical dynamics. Elife 10:e69011.

Edelstein AD, Tsuchida MA, Amodaj N, Pinkard H, Vale RD, Stuurman N (2014) Advanced methods of microscope control using μManager software. J Biol Methods 1:e10.

Epi PMC (2015) A roadmap for precision medicine in the epilepsies. Lancet Neurol 14:1219–1228.

Gilad A, Gallero-Salas Y, Groos D, Helmchen F (2018) Behavioral strategy determines frontal or posterior location of short-term memory in neocortex. Neuron 99:814–828.e7.

Goldey GJ, Roumis DK, Glickfeld LL, Kerlin AM, Reid RC, Bonin V, Schafer DP, Andermann ML (2014) Removable cranial windows for long-term imaging in awake mice. Nat Protoc 9:2515–2538.

Groppe D (2023) Bonferroni-Holm Correction for Multiple Comparisons. MATLAB Central File Exchange. Available at https://www.mathworks.com/matlabcentral/fileexchange/28303-bonferroni-holm-correction-for-multiple-comparisons.

Harris KD, Shepherd GM (2015) The neocortical circuit: themes and variations. Nat Neurosci 18:170–181.

Hatcher A, Yu K, Meyer J, Aiba I, Deneen B, Noebels JL (2020) Pathogenesis of peritumoral hyperexcitability in an immunocompetent CRISPR-based glioblastoma model. J Clin Invest 130:2286–2300.

Helbig I, Tayoun AA (2016) Understanding genotypes and phenotypes in epileptic encephalopathies. Mol Syndromol 7:172–181.

Heron SE, Smith KR, Bahlo M, Nobili L, Kahana E, Licchetta L, Oliver KL, Mazarib A, Afawi Z, Korczyn A, Plazzi G, Petrou S, Berkovic SF, Scheffer IE, Dibbens LM (2012) Missense mutations in the sodium-gated potassium channel gene KCNT1 cause severe autosomal dominant nocturnal frontal lobe epilepsy. Nat Genet 44:1188–1190.

Jacobs EAK, Steinmetz NA, Peters AJ, Carandini M, Harris KD (2020) Cortical state fluctuations during sensory decision making. Curr Biol 30:4944–4955.e7.

Kim TH, Zhang Y, Lecoq J, Jung JC, Li J, Zeng H, Niell CM, Schnitzer MJ (2016) Long-term optical access to an estimated one million neurons in the live mouse cortex. Cell Rep 17:3385–3394.

Kramer MA, Cash SS (2012) Epilepsy as a disorder of cortical network organization. Neuroscientist 18:360–372.

Kullmann DM, Moreau AW, Bakiri Y, Nicholson E (2012) Plasticity of inhibition. Neuron 75:951–962.

Liou JY, Ma H, Wenzel M, Zhao M, Baird-Daniel E, Smith EH, Daniel A, Emerson R, Yuste R, Schwartz TH, Schevon CA (2018) Role of inhibitory control in modulating focal seizure spread. Brain 141:2083–2097.

Lynch M, Sutula T (2000) Recurrent excitatory connectivity in the dentate gyrus of kindled and kainic acid-treated rats. J Neurophysiol 83:693–704.

Madisen L, et al. (2015) Transgenic mice for intersectional targeting of neural sensors and effectors with high specificity and performance. Neuron 85:942–958.

Makino H, Ren C, Liu H, Kim AN, Kondapaneni N, Liu X, Kuzum D, Komiyama T (2017) Transformation of cortex-wide emergent properties during motor learning. Neuron 94:880–890.e8.

Martinez-Espinosa PL, Wu J, Yang C, Gonzalez-Perez V, Zhou H, Liang H, Xia XM, Lingle CJ (2015) Knockout of Slo2.2 enhances itch, abolishes KNa current, and increases action potential firing frequency in DRG neurons. Elife 4:e10013.

McTague A, Howell KB, Cross JH, Kurian MA, Scheffer IE (2016) The genetic landscape of the epileptic encephalopathies of infancy and childhood. Lancet Neurol 15:304–316.

Mikati MA, Jiang YH, Carboni M, Shashi V, Petrovski S, Spillmann R, Milligan CJ, Li M, Grefe A, McConkie A, Berkovic S, Scheffer I, Mullen S, Bonner M, Petrou S, Goldstein D (2015) Quinidine in the treatment of KCNT1-positive epilepsies. Ann Neurol 78:995–999.

Møller RS, et al. (2015) Mutations in KCNT1 cause a spectrum of focal epilepsies. Epilepsia 56:e114–e120.

Montgomery MK, Kim SH, Dovas A, Zhao HT, Goldberg AR, Xu W, Yagielski AJ, Cambareri MK, Patel KB, Mela A, Humala N, Thibodeaux DN, Shaik MA, Ma Y, Grinband J, Chow DS, Schevon C, Canoll P, Hillman EMC (2020) Glioma-induced alterations in neuronal activity and neurovascular coupling during disease progression. Cell Rep 31:107500.

Musall S, Kaufman MT, Juavinett AL, Gluf S, Churchland AK (2019) Single-trial neural dynamics are dominated by richly varied movements. Nat Neurosci 22:1677–1686.

Natan A (2021) Fast 2D peak finder. MATLAB Central File Exchange. Available at https://www.mathworks.com/matlabcentral/fileexchange/37388-fast-2d-peak-finder.

Noebels J (2017) Precision physiology and rescue of brain ion channel disorders. J Gen Physiol 149:533–546.

Oh SW, et al. (2014) A mesoscale connectome of the mouse brain. Nature 508:207–214.

Ohba C, et al. (2015) De novo KCNT1 mutations in early-onset epileptic encephalopathy. Epilepsia 56:e121–e128.

Pinto L, Rajan K, DePasquale B, Thiberge SY, Tank DW, Brody CD (2019) Task-dependent changes in the large-scale dynamics and necessity of cortical regions. Neuron 104:810–824.e9.

Plazzi G, Tinuper P, Montagna P, Provini F, Lugaresi E (1995) Epileptic nocturnal wanderings. Sleep 18:749–756.

Polack PO, Guillemain I, Hu E, Deransart C, Depaulis A, Charpier S (2007) Deep layer somatosensory cortical neurons initiate spike-and-wave discharges in a genetic model of absence seizures. J Neurosci 27:6590–6599.

Rakhade SN, Shah AK, Agarwal R, Yao B, Asano E, Loeb JA (2007) Activity-dependent gene expression correlates with interictal spiking in human neocortical epilepsy. Epilepsia 48 [Suppl 5]:86–95.

Ratzlaff EH, Grinvald A (1991) A tandem-lens epifluorescence macroscope: hundred-fold brightness advantage for wide-field imaging. J Neurosci Methods 36:127–137.

Rizzi S, Knaus HG, Schwarzer C (2016) Differential distribution of the sodium-activated potassium channels slick and slack in mouse brain. J Comp Neurol 524:2093–2116.

Rossi LF, Wykes RC, Kullmann DM, Carandini M (2017) Focal cortical seizures start as standing waves and propagate respecting homotopic connectivity. Nat Commun 8:217.

Rossi LF, Kullmann DM, Wykes RC (2018) The enlightened brain: novel imaging methods focus on epileptic networks at multiple scales. Front Cell Neurosci 12:82.

Salkoff DB, Zagha E, McCarthy E, McCormick DA (2020) Movement and performance explain widespread cortical activity in a visual detection task. Cereb Cortex 30:421–437.

Saunders A, Macosko EZ, Wysoker A, Goldman M, Krienen FM, de Rivera H, Bien E, Baum M, Bortolin L, Wang S, Goeva A, Nemesh J, Kamitaki N, Brumbaugh S, Kulp D, McCarroll SA (2018) Molecular diversity and specializations among the cells of the adult mouse brain. Cell 174:1015–1030.e6.

Scharfman HE, Sollas AL, Berger RE, Goodman JH (2003) Electrophysiological evidence of monosynaptic excitatory transmission between granule cells after seizure-induced mossy fiber sprouting. J Neurophysiol 90:2536–2547.

Shao LR, Dudek FE (2004) Increased excitatory synaptic activity and local connectivity of hippocampal CA1 pyramidal cells in rats with kainate-induced epilepsy. J Neurophysiol 92:1366–1373.

Shore AN, Colombo S, Tobin WF, Petri S, Cullen ER, Dominguez S, Bostick CD, Beaumont MA, Williams D, Khodagholy D, Yang M, Lutz CM, Peng Y, Gelinas JN, Goldstein DB, Boland MJ, Frankel WN, Weston MC (2020) Reduced GABAergic neuron excitability, altered synaptic connectivity, and seizures in a KCNT1 gain-of-function mouse model of childhood epilepsy. Cell Reports 33:108303.

Smith EH, Schevon CA (2016) Toward a mechanistic understanding of epileptic networks. Curr Neurol Neurosci Rep 16:97.

Steinmetz NA, Peters AJ (2019) widefield. GitHub. Available at https://github.com/nsteinme/steinmetz-et-al-2019.

Steinmetz NA, et al. (2017) Aberrant cortical activity in multiple GCaMP6-expressing transgenic mouse lines. eNeuro 4:ENEURO.0207-17.2017.

Turner TJ, Zourray C, Schorge S, Lignani G (2021) Recent advances in gene therapy for neurodevelopmental disorders with epilepsy. J Neurochem 157:229–262.

Valentín A, Anderson M, Alarcón G, Seoane JJ, Selway R, Binnie CD, Polkey CE (2002) Responses to single pulse electrical stimulation identify epileptogenesis in the human brain in vivo. Brain 125:1709–1718.

Wang Q, et al. (2020) The Allen mouse brain common coordinate framework: a 3D reference atlas. Cell 181:936–953.e20.

Wekselblatt JB, Flister ED, Piscopo DM, Niell CM (2016) Large-scale imaging of cortical dynamics during sensory perception and behavior. J Neurophysiol 115:2852–2866.

Williams MS, Altwegg-Boussac T, Chavez M, Lecas S, Mahon S, Charpier S (2016) Integrative properties and transfer function of cortical neurons initiating absence seizures in a rat genetic model. J Physiol 594:6733–6751.

Yuan A, Santi CM, Wei A, Wang ZW, Pollak K, Nonet M, Kaczmarek L, Crowder CM, Salkoff L (2003) The sodium-activated potassium channel is encoded by a member of the Slo gene family. Neuron 37:765–773.

Zatka-Haas P, Steinmetz NA, Carandini M, Harris KD (2021) Sensory coding and the causal impact of mouse cortex in a visual decision. Elife 10:e63163.

Zaveri HP, Schelter B, Schevon CA, Jiruska P, Jefferys JGR, Worrell G, Schulze-Bonhage A, Joshi RB, Jirsa V, Goodfellow M, Meisel C, Lehnertz K (2020) Controversies on the network theory of epilepsy: debates held during the ICTALS 2019 conference. Seizure 78:78–85.

Zeisel A, Hochgerner H, Lönnerberg P, Johnsson A, Memic F, van der Zwan J, Häring M, Braun E, Borm LE, La Manno G, Codeluppi S, Furlan A, Lee K, Skene N, Harris KD, Hjerling-Leffler J, Arenas E, Ernfors P, Marklund U, Linnarsson S (2018) Molecular architecture of the mouse nervous system. Cell 174:999–1014.e22.